Biointerface Research in Applied Chemistry
Open-Access Journal (ISSN: 2069-5837)

Review
Volume 13, Issue 6, 2023, 555
https://doi.org/10.33263/BRIAC136.555

Selective Binding of Bovine Serum Albumin (BSA): A Comprehensive Review

Sunita Behera [1], Patitapaban Mohanty [1], Pragyan Parimita Dash [1], Pooja Mohapatra [1], Lipsa Shubhadarshinee [1], Rubi Behura [1], Aruna Kumar Barick [1], Priyaranjan Mohapatra [1], Bigyan R. Jali [1,*]

[1] Department of Chemistry, Veer Surendra Sai University of Technology, Burla, Sambalpur, Odisha, India
* Correspondence: bigyan.Jali7@gmail.com (B.R.J.);

Scopus Author ID 36503969200
ORCID ID:
Received: 1.11.2022; Accepted: 7.01.2023; Published: 24.02.2023

Abstract: Numerous complexes have been synthesized and characterized as the result of the ongoing search for novel molecules with potent therapeutic properties. These compounds have been shown to have potential applications as pharmacological agents due to their antibacterial, antiviral, antifungal, anticancer, and antineoplastic properties. The study of the coordination compound's affinity for this family of proteins as well as a knowledge of the mechanism by which they interact is essential due to the significant role that serum albumin plays in the pharmacokinetics and pharmacodynamics of medications. This review will concentrate on the composition of Schiff base, Schiff base metal complexes, various drug derivatives, nanoparticles, quinoline derivatives, and imidazolium-based salt derivatives that can bind to bovine serum albumin (BSA), its structural and biological rules, as well as various experimental techniques like UV-Vis absorption, Fluorescence, Dynamic light scattering (DLS), Circular dichroism (CD) and computational methods like molecular docking studies are used to investigate and assess these interactions.

Keywords: BSA interaction; coordination complex; fluorescence spectroscopy; UV-Vis absorption spectroscopy; molecular docking study.

1. Introduction

Albumin is a single polypeptide produced in the liver. It has the most prevalent soluble extracellular protein of the circulatory system, which makes up 60% of all the serum in mammals and is crucial for controlling blood pressure and pH [1]. The most normally employed protein models in biophysical and biochemical research in recent years are BSA and HSA, which share 76% of their similarity [2]. BSA has 582 amino acid residues, 20 tyrosyl residues (Tyr), and two tryptophan residues (Try), which are situated in positions 134 (sub-domain IA) and 212 (sub-domain IIA), according to the analysis of the crystal structure [3]. Compared to other extracellular proteins, serum albumin's basic structure is unique. One cysteine group (Cys-34) and a little tryptophan are present in serum albumin. According to X-ray crystallography examinations [4,5], the secondary structure has 17 disulfide bridges, 9 loops, and nearly 67% helix, leading to a heart-shaped 3D structure [6]. The three domains I, II, and III that make up the tertiary structure are separated into two subdomains, A and B, for each domain. It can be characterized as a particularly flexible protein that adapts to changes in its external environment and the binding of ligands. Despite this, albumin has a strong structure that can instantly restore shape according to the disulfide bridges, which is incredibly beneficial

in physiological situations. Since serum albumin is the most prevalent protein in blood plasma and typically has a concentration of 50 g/L, it has received the most research attention. Human serum albumin (HSA), bovine serum albumin (BSA), rat serum albumin (RSA), and equine serum (ESA) are some of the albumins that are most frequently researched. It has been discovered that serum albumins are crucial for several biological processes, including a) the maintenance of colloid osmotic pressure (COP): albumin is responsible for 75-80% of the blood's osmotic pressure. It is the primary protein in the interstitial fluid and the plasma. It describes the fluid flow inside and outside the capillaries [7]; (b) binding and transport, particularly of drugs: By attaching to it, albumin facilitates the delivery of medicines and ligands and lowers serum levels accumulating these components. Albumin has specifically four binding sites with distinct degrees of selectivity for various compounds. Competitive drug binding is possible, causing conformational modifications at the same site or distinct regions, such as warfarin and valium. They can therefore be regarded as carriers for a variety of exogenous and endogenous substances [4,5]; (c) Free radical scavenging: Sulfhydryl groups, or "thiols," are found primarily in albumin, and they scavenge free radicals (species of nitrogen and oxygen) [7]. (d) Acid-base balance: A protein with a high concentration of negative charge called albumin can be found in plasma. This strongly influences what is known as the "anion gap": Anions' and cations' concentrations in plasma should be equal. Albumin provides most of the remaining anions inorganic phosphate and hemoglobin [7]; (e) Effects on vascular permeability: When subjected to stress, albumin helps prevent capillary bed leakage due to a rise in the permeability of the capillaries. This pertains to endothelial cells' ability to manage the gaps between their walls and their permeability. Albumin could block because of its negative charge where the gap has diverting effect. Due to this, colloids are useful for preserving vascular architecture [7]. So to develop therapeutic applications and biomedical applications like antimicrobial [8-11], antibacterial [12-14], anticancer [15-17], and antioxidant [18-22] activities against human cells, it is crucial to study the interaction of BSA with other compounds.[23-25]

1.1. Structure of Bovine Serum Albumin (BSA).

The primary structure of BSA was speculated to consist of 585 residues, including amino acids. The bridges produce nine loops as a result of the sequence's 17 disulfide bonds. BSA is comparable to HSA in that it has 8 pairs of disulfide bonds and 1 cysteine [26], along with the four amino acid residues that have been eventually identified as belonging to the sequence Gly-Phe-Gln-Asn. BSA also includes significant amounts of Asp, Glu, Ala, Leu, and Lys [27]. The structural characteristics of BSA support the three homologous domains that make up the amino acid sequence [27,28]. According to circular dichroism measurements, the relative amounts of the BSA secondary structures α-helix, β-sheet, turn, and random coil are 48.7%, 0%, 10.9%, and 30.7%, respectively [27-35]. It has been proposed that the α-helices in the secondary structure of BSA are consistently distributed in the subdomains and the linkages between the domains. While the intra-domain hinge portions primarily have a non-helical structure, most residues in the long loops (apart from at the end) and the sections connecting the domains may form helices. The structure's fundamental building blocks are the subdomain's three lengthy helices. These connect to each other. These run parallel, and a trough is produced because the central helix (Y) is placed a little lower than usual. The spiral disulfide bridges serve as the principal connecting processes [36-44].

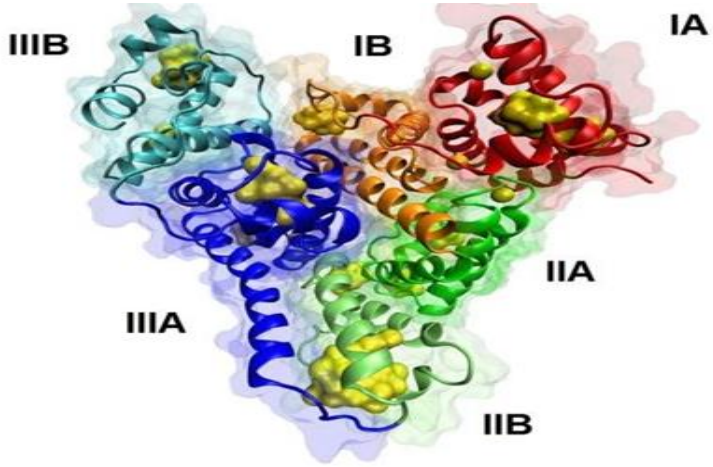

Figure 1. A BSA model structure based on the HSA Xray crystal structure found in the Protein Data Bank (PDB ID: 1UOR) is depicted using two side-on 3D graphics [4].

According to the suggested domains and subdomains found in the BSA, the 3D visual structure (Figure 1) agrees. It demonstrates the existence of two tryptophan residues, which serve as the primary catalyst for the intrinsic fluorescence of BSA [31].

2. Results and Discussion

Numerous active compounds are known to be involved in the recognition of proteins. We discuss numerous examples of Schiff base and its metal complexes, drug derivatives, nanoparticles, quinoline derivatives, and imidazolium-based salt derivatives.

2.1. Schiff base and its metal complexes interaction with BSA.

The C=N group containing Schiff base compounds show numerous biological and environmental application like antifungal, antiviral, and anticancer properties [45-47]. These Schiff bases play an essential role not only in medical and pharmaceutical industries but also in enzymatic reactions involving the interaction of the amino group of an enzyme, usually that of a lysine residue. Schiff base possesses heterocyclic rings with nitrogen, oxygen, and sulfur atom, which gives various activities like antibacterial, antimalarial, anti-inflammatory, and antipyretic [48]. Schiff base metal complexes have been employed in various applications, including catalysis, optics, electronics, antibacterial, antifungal, antiviral, anti-inflammatory, antioxidant, and anticancer [49-55]. The biological activity of metal was enhanced by Schiff base ligands interacting with metal ions based on co-ordination chemistry, but the importance of metal ions in medicine is substantial. Depending on reactivity and setup, the functional group of Schiff base and drug delivery action shows some beneficial role [56-57]. Due to their various spectral, molecular, and electrochemical properties, transition metal complexes have been researched as potential medications. Ping *et al*. synthesized a novel Schiff base 1 (Figure 2) and examined its interaction with BSA using various spectroscopic techniques [58]. From the fluorescence titration, the fluorescence peak of BSA was quenched at 354 nm due to the static mechanism. The stability of the BSA-1 complex was stabilized by hydrophobic forces and hydrogen bonds. The stable complex was also confirmed by Vent-Hoff parameters. The negative values of thermodynamic parameters (ΔH and ΔS) indicated stable interaction within the complex. The binding constant was calculated and found to be $2.169\times105\ M^{-1}$.

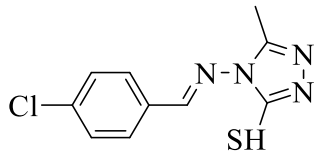

1

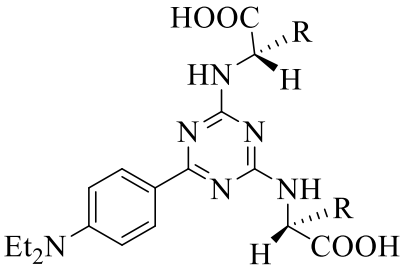

2a-e

a; R = H, **b**; R = CH_2SH, **c**; R = CH_2Ph,
d; R = p-OH-C_6H_4, **e**; R = 2-methyl indole

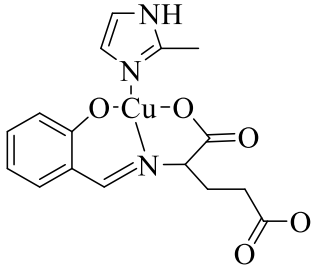

3a

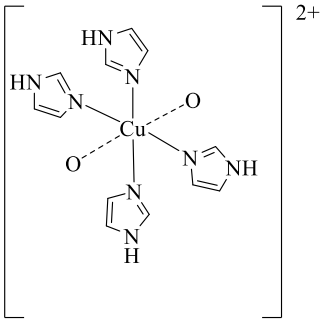

3b

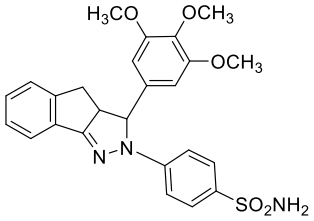

4

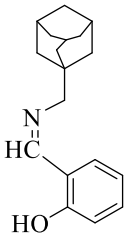

5a

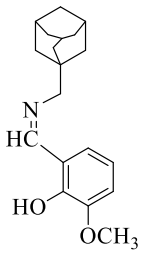

5b

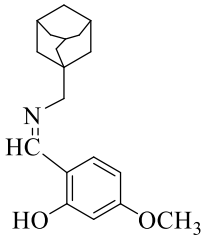

5c

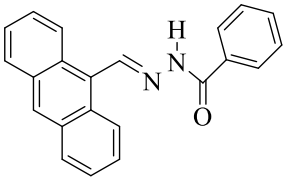

6a

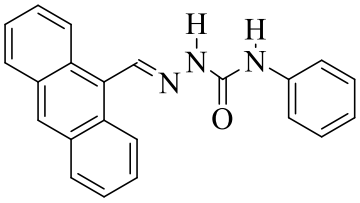

6b

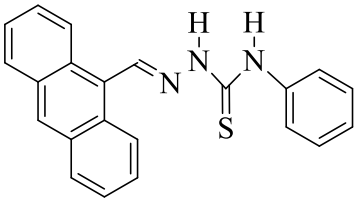

6c

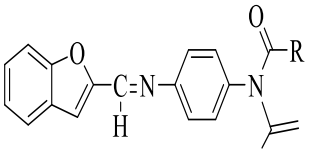

7a-g

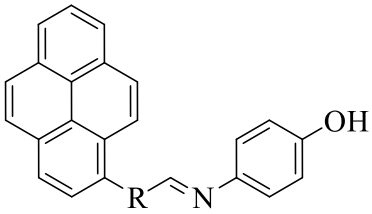

8a-b

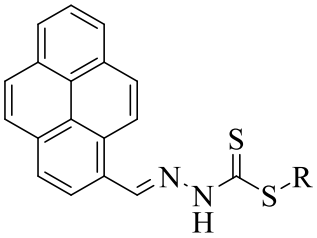

9a-b

7a: R = 2,5-difluorotoluene,
7b: R = toluene, **7c**: R = 4-nitrotoluene,
7d: R= 2,3,4-trifluorotoluene,
7e: R = 3,5-difluorotoluene,
7f: R= 4-methoxytoluene,
7g: R= 4-hydroxytoluene

8a: R = Thiophene, **8b**: R = Benzene

9a: R = CH_3,
9b: R = CH_2-Ph

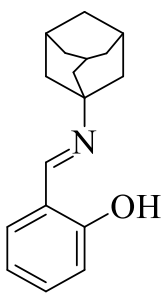

10a

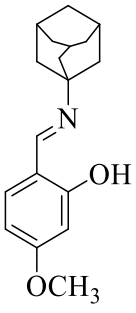

10b

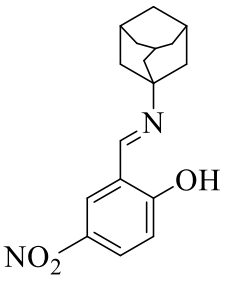

10c

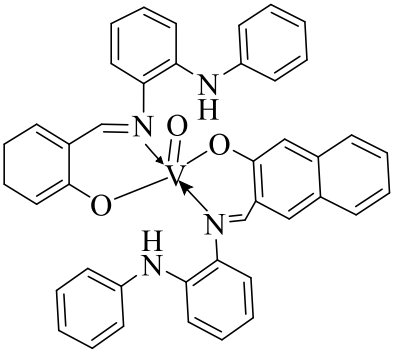

11a

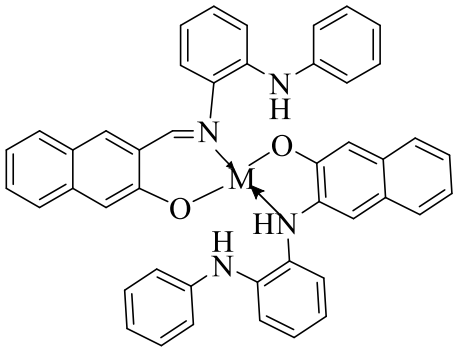

11b-c

11b: M = Cu (II), **11c**: M = Zn (II)

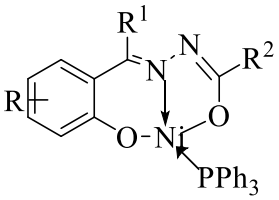

12a-d

12a: R = H, R^1 = H, R^2 = p-Me-C_6H_4

12b: R = H, R^1 = CH_3, R^2 = p-Me-C_6H_4

12c: R = H, R^1 = CH_3, R^2 = C_6H_5

12d: R = C_6H_5, R^1 = H, R^2 = C_6H_5

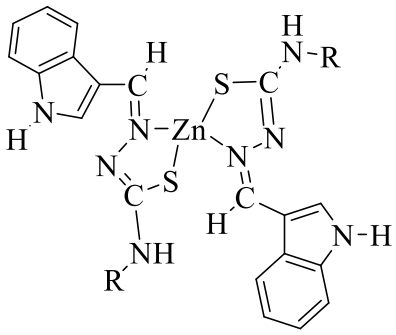

13a-d

13a: R = H, **13b**: R = CH_3**,**

13c: R = C_2H_5**, 13d**: R = C_6H_{11}

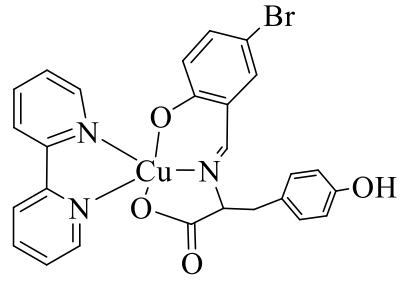

14a

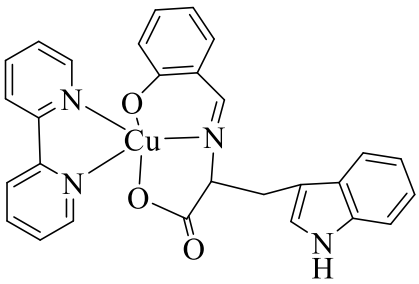

14b

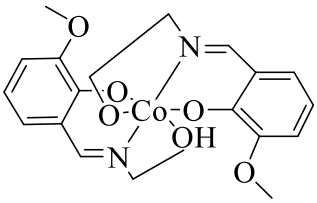

15a

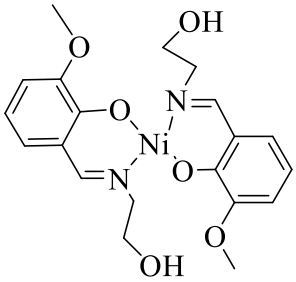

15b

Figure 2. Schiff base derivatives (1-15) as active binders of BSA.

Padalkar *et al*. designed and synthesized a series of novel Schiff base complexes 2a-e (Figure 2) [59]. These were further characterized by using various spectroscopic analyses. The UV-Vis absorption and emission spectra were recorded in the presence of DMSO, and it was observed that compounds 2a-e showed similar behaviors. The binding of all fluorophores with BSA depends upon conjugation and varying concentration. The fluorescence progressively declined upon conjugation and stabilized at a specific fluorophore concentration. The steady line in the graph suggested stability. It was observed that the carboxylic groups of the above derivatives attach to those of protein. A series of novel copper-containing Schiff base derivatives 3a-b (Figure 2) were designed and synthesized by Andrezalova *et al*. [60]. Various spectral analyses are used to characterize the interaction and binding properties. The absorption peaks obtained from UV-Vis spectra are in the region of 300-420nm. In fluorescence spectroscopy, the emission peak at 280 nm was seen to be quenched. The dynamic quenching was observed due to rapid hydrogen bonding. The calculated binding constants for complex 3a and 3b were 2.74×105 and 2.54×106, respectively. Further applications of the 3a and 3b

complexes were made against cancer cells. Bozkurt *et al*. designed and synthesized a novel pyrazoline-based Schiff base derivative 4 (Figure 2) and examined its binding properties through different spectroscopic analyses [61]. The interaction between BSA and 4 was analyzed through UV-vis absorption and fluorescence spectral analysis. In tris-HCl buffer, BSA displayed a weak absorption peak at 275 nm. The addition of 4 to BSA resulted in a new peak at 365 nm. The quenched fluorescence at 280 nm was observed due to static quenching. The binding process was observed to be spontaneous. The binding constants were calculated at different temperatures like 288K, 298K, 308K, and 318K, and were found to be 1.29×103, 0.91×103, 0.56×103 and 0.19×103 M^{-1}, respectively. Liu *et al*. synthesized a series of novel rimantadine-based Schiff base complexes 5a-c (Figure 2) and examined their binding behavior towards BSA through various spectral analyses [62]. The interaction with BSA was discovered to be hydrophobic. The addition of 5a-c to BSA; resulted in a static quenching in the fluorescence peak. However, when compounds 5a and 5b were added to BSA, the blue peak shifted to 337nm, and when compound 5c was added, the blue-shifted to 336 nm. It indicated the 5c-BSA complex's stable binding, with a binding constant of 16.029×104 M^{-1}. A series of anthracene-based Schiff base complexes 6a-c (Figure 2) were designed and synthesized by Densil *et al*. to investigate its binding interaction with BSA through several spectral techniques [63]. The fluorescence spectra of compounds 6a-c showed an emission peak in the range of 430-460 nm. The addition of 6a-c to BSA in buffer solution resulted in a continuous increase in fluorescence peak with redshift from 464 to 479 nm. The morphology of aggregation was also studied through SEM analysis. Due to the intense hydrogen bonds and hydrophobic interactions with BSA, the absorption intensity of 6a-c was blue-shifted. The calculation revealed that the binding constants for 6a-c were 1.8×105, 5.4 ×107, and 6.0×106 M^{-1}, respectively. The complexes of BSA-6a-c were applied for the cell imaging study. In order to analyze the binding behavior with BSA, Prashanth *et al*. designed and synthesized a series of novel benzamide-based Schiff base derivatives 7a-g (Figure 2) and characterized them through various spectral analyses [64]. BSA in buffer solution displayed quenched fluorescence at 340 nm in the presence of all the compounds 7a-g due to static quenching. The emission peak was red-shifted for 7b, 7e, and 7g and blue-shifted for 7a, 7d, and 7f. It attributed the suppression of polarity around tryptophan residue, which further increased hydrophobicity. Due to different molecular sizes and polarity, the binding constant of the 7g-BSA complex is high, among others. The binding constants are estimated and found to be 1.09×104, 2.59×104, 0.79×105, 1.57×105, 5.26×105 and 6.38×105 M^{-1}, respectively. Complex 7a, 7c, 7d, and 7e showed good antibacterial activities, while the 7a, 7d, and 7e exhibited good antifungal activities, and 7f and 7g displayed better antioxidant properties. Srinivasan *et al*. reported two novels pyrene-based Schiff base derivatives, 8a-b (Figure 2), and were being examined through various spectroscopic techniques to study their interaction with BSA [65]. The peak in the fluorescence spectra of BSA showed a static decline with increasing concentrations of 8a-b. It indicates the significant interaction within the Schiff base-BSA complexes. The binding constants were calculated and found to be 3.81×105 and 4.53×105 M^{-1}, respectively, for 8a and 8b. It was also established through molecular docking study that the amino acids of BSA and pyrene derivatives have created hydrophobic interactions. Also, some antibacterial and antimicrobial activities were examined. Sengottiyan *et al*. synthesized two novels pyrene-based Schiff base complexes 9a-b (Figure 2), and their binding properties were studied through different spectroscopic techniques [66]. The binding interaction was strong and was observed to be static. The binding constant of 9a-b complexes was evaluated and found to be 7.39×105 and

7.81×105 M^{-1}, respectively. The hydrophobic interactions and hydrogen bonds played an essential role in forming stable complexes between pyrene derivatives and BSA. The stable binding interaction was further confirmed from molecular docking analysis at physiological pH=7.1. Although complex 9b experienced a more dominant interaction than complex 9a due to a higher binding affinity and a lower binding energy value. Due to dynamic interaction, the quenched fluorescence was observed for both 9a and 9b. Niu *et al*. reported a series of new amantadine Schiff base complexes 10a-c (Figure 2) and used many spectroscopic techniques to analyze their interaction with BSA. BSA IN the Tris-HCl buffer displayed an emission peak at 340 nm due to intrinsic fluorescence [67]. Adding 10a-c to BSA in the buffer resulted in a quenched fluorescence due to static and dynamic interaction. The binding constant was observed to be high in 10b with BSA among the others and found to be 29.833×104 M^{-1}. A series of unique Schiff base metal complexes 11a-c (Figure 2) were designed and synthesized by Gurusamy *et al*. to examine their binding capabilities with BSA in buffer solution [68]. The UV-visible, fluorescence, and molecular docking studies showed that all the complexes showed a stronger affinity towards DNA, BSA, and HSA. The absorption band at 415 nm 445 nm increased with the addition of 11a and 11c; however, when 11b was added to the BSA, the absorption band shrank, and a new bond with two distinct isosbestic points at 355 nm, 344 nm, and 374 nm respectively. On the other hand, the fluorescence emission was reduced when all the complexes were added to the BSA. The binding constants were calculated and found to be 1.19 × 104, 1.44 × 104, and 7.66 × 103 M^{-1}, respectively. All the metal complexes showed excellent antibacterial and antioxidant activity against bacteria. Four new bivalent nickel-derived Schiff base complexes 12a-d (Figure 2) were developed and reported by Sathyadevi *et al*. [69]. The compounds 12a-d were further characterized by various spectral approaches to analyze their interaction with BSA. The absorption spectra were seen in the range of 200-470 nm, but due to mechanisms involving ligand-to-metal charge transfer (LMCT) and metal-to-ligand charge transfer (MLCT), the strong absorption band was produced between 250 and 300 nm. The fluorescence emission intensity dropped statically with a hypsochromic shift of 2 nm after adding 12a-d. It indicates the aggregation of BSA with Ni complexes. The antioxidant and cytotoxicity properties of these complexes were studied as potential therapeutic targets. A series of novel Schiff base-zinc complexes 13a-d (Figure 2) was devised by Balakrishnan *et al*., and their binding behavior with BSA was investigated using various spectrophotometric techniques [70]. The quenched fluorescence at 345 nm was observed in fluorescence spectra. When complexes 13a-d were added, the peak was significantly decreased and redshifted to demonstrate the BSA's functional interaction. It was analyzed that complex 13d interacts with BSA more strongly than the other complexes due to its high binding constant of 1.592×106 M-1. The addition of 13a-d to the BSA caused a conformational change in the environment of BSA, i.e., a red shift of the emission peak in fluorescence spectra was detected due to the static mode of quenching. The molecular docking analysis confirmed the complex's hydrogen bonding and hydrophobic interactions. The synthesized 13d complex of zinc showed tumor selectivity for the A549 cancer cell with a lower I50 value in cytotoxicity experiments.Two novel ternary copper (II) Schiff base complexes 14a and 14b (Figure 2) were demonstrated by Dezhampanah *et al*. to be active binders of BSA in the buffer [71]. The quenched fluorescence peak of BSA was observed upon adding 14a and 14b due to the static quenching mood. The change in spectral behavior signified the stable complexation. Docking studies confirmed that both 14a and 14b aggregates with the tryptophan moiety of BSA through hydrogen and van der Waals forces stabilize the complex formations. All spectroscopic studies showed that the

complex 14b has a stronger binding affinity than 14a, which was beneficial in medical applications. The novel metal complexes of Schiff base 15 (Figure 2) were devised by Keshavarzian *et al*. [72]. The interaction of metal complexes with BSA was studied through various spectroscopic tools. Both fluorescence emission and UV-vis absorption spectral analysis suggested that the interaction of both metal complexes of 15 with BSA involves a static quenching process. From the molecular docking studies, it was found that both the metal complexes interact hydrophobically with BSA. Co (III) complexes are significantly less capable of binding than Ni (II) complexes. Ni (II) complex displayed active anticancer and antibacterial properties.

Table 1. Selective parameters of Schiff base derivatives as active binders of BSA.

Receptor	Solvent	Binding Constant (M^{-1})	Mechanism	Application	Reference
1	Phosphate buffer solution (PBS)	2.169×10^5	Static Quenching	Insight into physiological study of BSA.	[58]
2	Phosphate buffer solution (PBS)	---	Static Quenching	---	[59]
3	Phosphate buffer solution (PBS)	2.74×10^5, 2.54×10^6	Dynamic quenching	Anti-cancer activities	[60]
4	Tris HCl Buffer	0.91×10^3	Static Quenching	Vitro model study	[61]
5	Tris HCl-NaCl Buffer	3.251×10^4 2.749×10^4 16.029×10^4	Static Quenching	---	[62]
6	Phosphate buffer solution (PBS)	1.8×10^5, 5.4×10^7, 6.0×10^6	Hydrophobic Interaction	Cell imaging	[63]
7	Tris HCl Buffer	1.09×10^4, 2.59×10^4, 0.79×10^5, 1.57×10^5, 5.26×10^5, 6.38×10^5	Static Quenching	Anti-oxidant activities, Anti-microbial activities	[64]
8	Phosphate buffer solution (PBS)	3.81×10^5 4.53×10^5	Static Quenching	Anti-bacterial activities	[65]
9	Phosphate buffer solution (PBS)	7.39×10^5 7.81×10^5	Dynamic quenching	Anti-biotic activities	[66]
10	Tris HCl Buffer	7.26×10^3 7.64×10^3 9.75×10^3	Static and Dynamic quenching	Toxic study	[67]
11	Phosphate buffer solution (PBS)	1.19×10^4 1.44×10^4 7.66×10^3	Static Quenching	Anti-oxidant and Anti-bacterial activities	[68]
12	Phosphate buffer solution (PBS)	5.670×10^5 8.300×10^5 1.221×10^6 1.086×10^7	Static and Dynamic quenching	Anti-oxidant and Cytotoxicity activities	[69]
13	Phosphate buffer solution (PBS)	1.898×10^4 7.720×10^5 8.302×10^5 1.592×10^5	Static Quenching	*In vitro* cytotoxicity and Anti-cancer studies	[70]
14	Phosphate buffer solution (PBS)	0.67×10^5 2.02×10^5	Static Quenching	Drug design and Medical communication	[71]
15	Tris HCl Buffer	7.5×10^2 1.0×10^3	Static Quenching	Antibacterial and anticancer study	[72]

2.2. Interaction of drugs with BSA.

The association between coordination compounds and plasma proteins has been defined by studies on pharmaceutical design and pharmacology [73]. Drug interactions at the protein binding level would significantly impact the apparent drug distribution volume and the drug

clearance rate. Therefore, understanding how pharmaceuticals are carried and dispersed throughout the body as well as revealing their modes of action and pharmacological dynamics, required research into the interactions between medications and serum albumins [74-76] On this aspect, a newly discovered triazolobenzenediazepine drug 16 (Figure 3) that acts as a sedative and hypnotic agent was reported by Zhang *et al*. and characterize its binding features with BSA using various spectroscopic analysis [77]. When the drug derivative 16 was combined with BSA in a buffer solution, the fluorescence emission peak was statically quenched. It confirms the complex formation with BSA. On the other hand, adding 16 to the BSA also resulted in a red shift in the absorption band at 206 nm. The binding affinity of the 16-BSA complex was stabilized due to the hydrophobic interaction. Further, the complex was applied in various pharmacological applications due to its unique binding property.

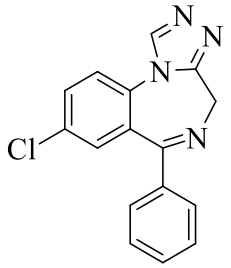

16

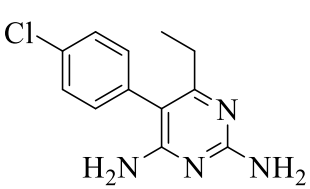

17a

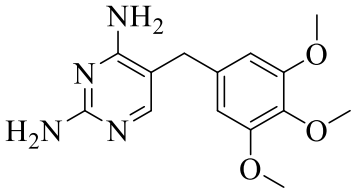

17b

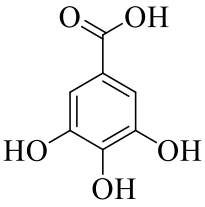

18

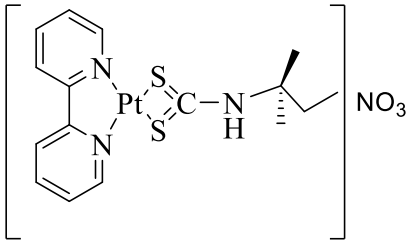

19

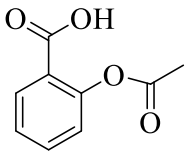

20a

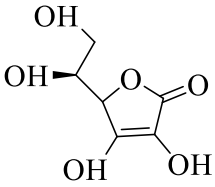

20b

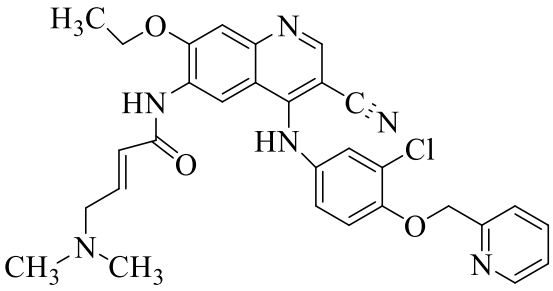

21

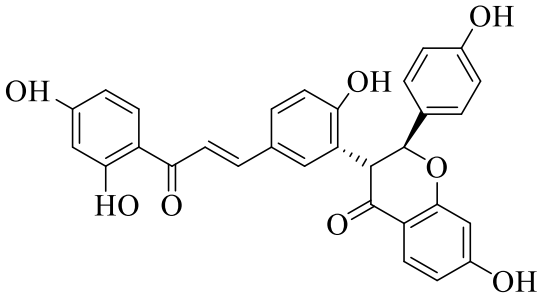

22

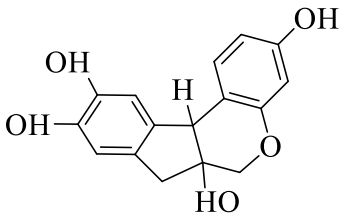

23

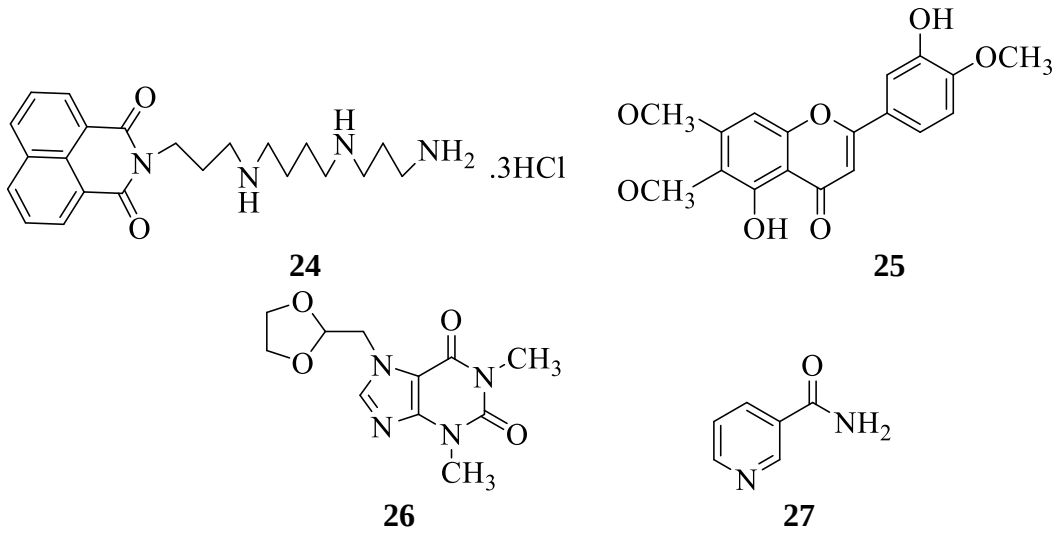

Figure 3. Various drugs (16-27) as active binders of BSA.

Sun *et al*. discovered a series of novel coccidiosis 17a-b (Figure 3) and described their binding interaction with BSA through several spectral techniques and molecular docking studies [78]. From the fluorescence titration, a static quenching of the peak was obtained to gather information about the stability of the BSA-17 complex. Thermodynamic and electrostatic forces are the main cause of binding. Due to red-shift, the static quenching in the fluorescence peak was observed at 306 for 17a and 304 for 17b. The molecular docking analysis confirmed the hydrophobic interactions with BSA. The complexes have a wide range of pharmacological and physiological effects based on their interaction with BSA. Khatun *et al*. reported a novel drug 18 (Figure 3) and studied its properties and binding ability with BSA using different spectroscopic instruments and molecular docking studies [79]. The observed static quenching mechanism in fluorescence titration points to the development a complex between 18 and BSA, which has a binding constant of 2.19×104 M^{-1}. The emission peak at 344nm was gradually dropped with an increasing concentration of 18. The interaction occurring at site I (subdomain II A) was van der Waals forces of interaction, shown through molecular docking studies. The 18-BSA complex exhibited various pharmacological properties, including antioxidant, anticarcinogenic, antifungal, and anti-inflammatory activities. Shiraz *et al*. devised an anticancer drug 19 (Figure 3) and investigated its interaction ability through molecular docking analysis and binding properties through various spectroscopic techniques [80]. According to the thermodynamic parameter analysis, Vander Waal and hydrogen bonding interactions were the primary binding forces. Fluorescence titration resulted in a static quenching of a peak at 345 nm when the concentration of 19 was increased. It indicates the formation of a stable complex with a binding constant of 3.99×104 M^{-1}. The molecular docking studies demonstrated that compound 19 alters the polarity and surrounding space of the protein to attach to it. With fewer adverse effects, the aforementioned compound was more effective against a select form of cancer. A series of novel compounds 20a–b (Figure 3) were reported by Nafisi *et al*., and their binding interaction was studied using a variety of spectroscopic techniques [81]. Upon increased concentration, the UV-vis absorption peaks of BSA were obtained at 255nm for 20a and 273nm for 20b. Both compounds interact hydrophilically with BSA and contain polar amino groups. The binding constants were calculated and found to be 1.57×104 M^{-1} and 1.15×104 M^{-1} for 20a and 20b, respectively. These compounds have inherent antioxidant and anti-inflammatory properties. Probe 21 (Figure 3) was devised by Wani *et al*., characterized its properties through various

spectroscopic instruments, and studied its binding ability by molecular docking analysis [82]. From fluorescence titration, the emission peak of BSA was observed at 350nm, and it statically decreased with an increasing concentration of 21. It attributed the formation of a complex with a binding constant of 8.1×104 M-1. Vander Waals and hydrogen bonding at site I (subdomain II) of BSA were responsible for the stability of that complex. The complex was further applied for anti-cancer drugs study and human breast cancer treatment. With the use of molecular docking studies and other spectroscopic analyses, Chaves *et al*. described the binding interaction of BSA with a novel drug 22 (Figure 3) [83]. The interaction between BSA and 22 was mainly lipophilic, attributed to the negative value of thermodynamic parameters. The quenched fluorescence emission was observed at 340 nm in fluorescence titration analysis. The molecular docking studies showed that Trp- 213 was the major binding site where lipophilic and hydrogen bonding interactions occurred. These drugs showed important biological activities like antitumor, cytotoxicity, antiviral, and antimicrobial. Patel *et al*. reported a novel drug, 23 (Figure 3), and investigated its comparative effect on BSA through various spectral techniques and molecular analysis [84]. The absorption spectrum of BSA was observed at 279 nm. The regular decrease in the intensity of absorption peak upon adding 23 indicates the formation of the complex. The quenched fluorescence at 345 nm was observed due to the static mode of quenching. According to molecular docking studies, it was found that the interaction was Vander Waals and electrostatic forces of interaction. The binding constant was calculated and found to be 2.78×104 M-1. In addition to being used in pharmaceutical applications, the binding mechanism helps in comparative research of antihistamine drugs. In order to comprehend the binding sites of BSA with the drug, Tiana *et al*. reported a novel drug 24. (Figure 3) [85]. The quenched fluorescence of BSA was observed due to the static quenching mechanism. It indicates the effective 25 and BSA. The hypochromic shift in the absorption spectrum and molecular docking studies confirmed the hydrophobic interaction at site II of BSA. Xu *et al*. reported a new drug 25 (Figure 3) and examined its protein interactions using various spectroscopic techniques [86]. The absorption peak of BSA was observed at 220 nm, and upon adding 25, a slight redshift of about 2 nm was observed. The quenched fluorescence of BSA at 340 nm was observed in the presence of 25 due to static quenching mode. It confirms the interaction of BSA with 25. The hydrophobic and electrostatic forces were responsible for the stability of the complex. Thermodynamic, temperature-dependent parameters estimated the binding forces to be hydrophobic and electrostatic forces to stabilize the BSA-25 complex. Drug-protein interactions that lead to antiproliferative effects in tumor cells have an impact on the pharmacological effects of drugs. A novel drug 26 (Figure 3) was discovered by Siddiqui *et al*., and their characteristics were observed using several spectroscopic tools [87]. A quenching in the fluorescence emission peak of BSA was observed at 340 nm, and the absorption intensity was seen to be enhanced at 278 nm in the presence of 26. The change in spectral behavior has been attributed to forming of the BSA-26 complex. According to thermodynamic and computational analysis, the main forces that caused stable complexation were hydrogen, hydrophobic, and van der Waals forces. It was further validated through molecular docking analysis also. These binding ability investigations offered some pharmacological activities, such as asthma therapy. Gu *et al*. reported a novel drug 27 (Figure 3) that reduces hyperlipidemia and studied its binding interaction using several spectroscopic techniques [88]. The emission peak of BSA in buffer solution was found to be at 345 nm, and as the concentration of 27 was increased, a quenching in the peak was observed, showing the interaction between 27 and BSA. From the UV-vis titration analysis, the red shift in the

absorption band at 210 nm was observed due to the formation of the complex. According to molecular docking analysis, the hydrophobic cavity of BSA forms hydrophobic bonds with 27 with a binding constant of 2.19×103 M^{-1}. Thermodynamic parameters demonstrated that hydrophobic interactions drove spontaneous binding interactions. To treat the target organs, the metabolic potential of 27 was studied.

Table 2. Selective parameters of various drugs as an active binder of BSA.

Receptor	Solvent	Binding Constant (M^{-1})	Mechanism	Application	Reference
16	Tris-HCl buffer	4.977×10^{3}	Static quenching	Pharmaceutical application	[77]
17	Tris-HCl buffer	1.386×10^{4} 0.871×10^{4}	Static quenching	Pharmacological and Physiological	[78]
18	Sodium Phosphate buffer	2.19×10^{4}	Static or Dynamic Quenching	Pharmacological and Medicinal fields	[79]
19	Tris-HCl buffer	3×10^{8}	Static quenching	Anticancer activity	[80]
20	Tris buffer	1.57×10^{4} 1.15×10^{4}	Static or Dynamic Quenching	Vitro analysis	[81]
21	Phosphate buffer	8.1×10^{4}	Static quenching	Breast cancer	[82]
22	PBS buffer	4.89×10^{4}	Static or Dynamic Quenching	---	[83]
23	Tris buffer	2.18×10^{4}	Static quenching (Hydrophobic interaction)	Anti-amyloidogenic activity	[84]
24	Tris-HCl buffer	2.290×10^{5}	Static quenching (Hydrophobic interaction)	---	[85]
25	PBS buffer	1.679×10^{6}	Static quenching (Hydrophobic interaction)	---	[86]
26	Tris buffer	5.067×10^{3}	Static quenching	*In vitro* and *in silico* approach	[87]
27	Tris buffer solution	2.19×10^{3}	Dynamic quenching	Therapeutic drugs	[88]

2.3. Interaction of BSA with nanoparticles.

Nanoparticles of various sizes, morphologies, and surface chemistries have been developed due to developments in engineering, materials science, and nanotechnology [89]. The <100 nm nanoparticles have special size-dependent optical features, including enhanced photochemical stability, high quantum yield, broadband excitation, tunable emission wavelength, and symmetrical emission spectra [90-91]. For both *in vivo* and in vitro biomedical research and applications, the size of nanomaterials, similar to that of most biological molecules and structures, might be of tremendous value [92]. The nanoparticles involve metal nanoparticles, silica nanoparticles, and luminescence quantum dots [93]. Additionally, a variety of possible uses for them have been discovered in photovoltaic technology, medicine delivery, biological markers, and cellular imaging [94-96]. On that aspect, Prasad *et al.* synthesized a ZnO nanoparticle 28 from citrus lemon extract having an average dimension of 11 nm. They were applied to study its binding interaction with BSA through fluorimetric analysis [97]. The addition of 28 to the buffer solution of BSA resulted in a quenching in fluorescence intensity at 347 nm with a small blue shift of 4 nm. The change in spectral behavior was due to suppressing the hydrophobic part of the protein. From the molecular docking studies, the stability of the BSA-28 complex was confirmed. The binding constant was

calculated and found to be 1.05×1011 M^{-1}. The nanoparticle 28 was utilized as an antibacterial agent in the pharmacological field. A novel colloidal Ag nanoparticle 29 was reported by Ravindran *et al*. to study its binding iteration with BSA using UV-vis absorption study [98]. The Ag nanoparticle in deionized water showed two absorbance peaks at 425 nm and 280 nm in the absence of BSA. The addition of BSA displayed a continuous decrease in both the absorbance peak with a slight blue shift of 5-10 nm due to the conformational changes of BSA upon strong hydrophobic interaction with compound 29. The two novel hydrophobic and hydrophilic ferroferric oxide nanoparticles 30a and 30b were reported by Hao *et al*. to analyze their interaction with bovine serum albumin (BSA) [99]. From the fluorescence titration, the static quenching of the fluorescence peak was observed in both cases when the concentration of 30a and 30b were increased gradually. The change in spectral behavior implied the formation of a complex with BSA having binding constants 8.52 ×103 M^{-1} and 6.95×103 M^{-1} for 30a and 30b, respectively. The negative value of ΔH˚ and ΔS˚ signified the formation of the van der Walls interaction of intermolecular hydrogen bonding between BSA and 30b. By keeping the strategy of studying the interaction between BSA and nanoparticles, Esfandfar *et al*. reported a copper oxide nanoparticle 31, which can strongly bind with BSA in a buffer solution [100]. From the fluorescence spectral analysis, the quenched fluorescence for BSA was observed in the presence of 31 due to the conformational change of fluorophore position. The negative value of ΔH˚ and ΔS˚ also confirmed the hydrogen bonding interaction of 31 and BSA. The pyrimidine-based Schiff base copper nanoparticle 32 was reported by Jose *et al*. to serve as an active binding site for BSA [101]. The binding interaction of BSA with 32 was studied by various spectrophotometric analyses. The addition of 32 to the BSA in buffer solution resulted in an increase in absorption peak at 279 nm with a slight blue shift. The fluorescence spectroscopy analysis also revealed that the quenching in fluorescence of BSA was observed after the addition of 32 with a slight shift in wavelength due to the molecular interaction. The BSA-32 plays a lead role in antimicrobial, anticancer, and antioxidant drugs. The copper oxide-based nanoparticles 33 were designed and developed by Bhogale *et al*. to study their binding interaction with BSA [102]. The BSA in the buffer solution showed a strong fluorescence peak at 345 nm. The addition of 33 implied a static quenching in fluorescence spectra with a blue shift of 5 nm. The variation in the spectral behavior was due to the hydrogen bonding interaction within the BSA-33 complex. The negative value of thermodynamic parameters also signified the formation of a stable complex. The binding constant was calculated and found to be 5.01×106 M^{-1}. Boulos *et al*. reported a gold nanoparticle 34 to study its interaction with BSA through various spectrophotometric analyses and thermodynamic studies [103]. The fluorimetric analysis revealed that the quenching in fluorescence of BSA was observed after adding various concentrations of 34. The change in spectral behavior was due to the surface modification of BSA through Vander wall interaction. The thermodynamic parameter also signified the binding interaction within 34 and BSA. The binding constant of this interaction was calculated and found to be 2.75×1010 M-1. The polyethyleneimine functionalized ZnO nanoparticle 35 was synthesized by Chakraorti *et al*. to study its binding interaction with BSA through calorimetric and spectroscopic analysis [104]. The isothermal calorimetric titration data revealed the possibility of electrostatic interaction between BSA and 35. From the fluorescence analysis, it was also observed that the fluorescence spectrum of BSA was quenched after the addition of 35. The addition of 35 also resulted in a decrease in the absorbance peak of BSA. The change in spectral behavior was due to protein denaturation through hydrophobic interaction with 35. The binding constant was calculated and found to be

6.4×104 M-1. The BSA-35 complex was further utilized in various applications of nanotechnology. The pyrimidine-based Schiff base 36a and its corresponding nickel nanoparticle 36b were designed and synthesized by Jose *et al*. to study its BSA interaction, molecular docking, and antioxidant study [105]. The BSA in the buffer solution showed a weak absorption peak at 279 nm. The addition of 36a and 36b resulted in an increase in absorption peak at 279 nm. Similarly, adding 36a and 36b resulted in a quenching in fluorescence at 343 nm. The change in spectral behavior was mainly due to the hydrogen bonding and hydrophobic interaction within the 36a and 36b complexes of BSA. The binding constant was calculated and found to be 6.7×103 and 8.7×103 M-1 for 36a and 36b complex, respectively. The BSA ducking analysis also confirmed the formation of a stable complex with 36a and 36b. The BSA complex of 36a and 36b showed potent antibacterial, antimicrobial, and antioxidant activity. A new PVP-coated silver nanoparticle 37 was reported by Hashemnia *et al*. to study its influence on the binding of clonazepam to BSA through various spectrophotometric analyses and molecular docking studies [106]. Adding 37 to the HEPES buffer Solution of BSA displayed an increase in absorption peak at 279 nm. It indicates the adsorption of the BSA molecule on the surface of 37. On the other hand, adding 37 to BSA implied a quenching in the fluorescence of BSA. The binding constant was calculated and found to be 6.16×108 M-1. From the molecular docking analysis, the stability of hydrophobic interaction within the 37-BSA complex was confirmed. Mariam *et al*. reported a silver nanoparticle 38 to study its interaction with BSA through various spectrophotometric analyses [107]. The UV-vis titration found that adding 38 to BSA in buffer solution resulted in an increase in absorption peak at 279 nm with a slight blue shift of 2 nm. Further, adding 38 also resulted in a static quenching in fluorescence with a blue shift of 5 nm. Resonance light scattering spectra signified the formation of a complex between 38 and BSA. The calculated thermodynamic parameters also confirmed the hydrophobic interaction within the 38-BSA complex. The binding constant was estimated and found to be 1.716×1010 M-1. Juan *et al*. reported a gold nanoparticle 39 to study its interaction with BSA and the conformational changes of BSA after its complex formation with 39 [108]. This binding interaction study was analyzed by fluorescence spectrophotometric analysis. The fluorescence emission of BSA was quenched with the addition of 39. The static fluorescence quenching was due to the hydrophobic van der Walls interaction within the 39-BSA complex. The FTIR spectrum also confirmed the conformational change of the BSA surface after being complexed with 39. The binding constant of this stable complexation was calculated and found to be 7.59×108 M-1.

Table 3. Selective parameters of various nanoparticles as an active binder of BSA.

Receptor	Solvent	Binding Constant (M^{-1})	Mechanism	Application	Reference
28	Phosphate buffer	1.05×10^{11}	Static Quenching	Antibacterial agent	[97]
29	Deionized water	---	Hydrophobic interaction	---	[98]
30	Tris-HCl buffer	8.52×10^{3} 6.95×10^{3}	Static and dynamic Quenching	---	[99]
31	Phosphate buffer	---	Static Quenching	---	[100]
32	Tris-HCl buffer	1.92×10^{6}	Static Quenching	antimicrobial, anticancer, and antioxidant activity	[101]
33	Tris-HCl buffer	5.01×10^{6}	Static Quenching	---	[102]

Receptor	Solvent	Binding Constant (M^{-1})	Mechanism	Application	Reference
34	Phosphate buffer	2.75×10^{10}	Vander wall interaction	---	[103]
35	Phosphate buffer	6.4×10^{4}	Hydrophobic interaction	Application in nanotechnology	[104]
36	Tris-HCl buffer	6.7×10^{3} 8.7×10^{3}	Static Quenching	antibacterial, antimicrobial and antioxidant activity	[105]
37	HEPES buffer	6.16×10^{8}	Static and dynamic Quenching	Application in nanotechnology	[106]
38	Phosphate buffer	1.716×10^{10}	Static and dynamic Quenching	---	[107]
39	Tris-HCl buffer	7.59×10^{8}	Static Quenching	Pharmaceutical Application	[108]

2.4. Interaction of BSA with quinone moieties.

Quinones are widely dispersed substances in nature that have been found to exhibit a variety of pharmacological effects. Quinone also accelerates the different biochemical processes in the cells of living organisms. Various compounds based on quinones have biological properties, including herbicidal, fungicidal, algicidal, bacterial, etc. [109]. Quinonoid compounds are among the several natural and synthetic substances that have been tested for their ability to fight cancer [110]. Quinones' biological activity results from their acid-base characteristics and capacity to take one or two electrons. [111-112] The presence of substituents on either the quinone or the nearby rings significantly impacts the chemistry of quinone. Quinone toxicity is typically assumed to be caused by two mechanisms: first, as Michel acceptors, they harm living organisms by interacting with their cellular nucleophiles and causing protein alkylation. Reactive oxygen species are produced second as a redox agent [113-116]. Therefore it is an interesting and crucial subject to research what happens when quinones and serum albumin interact physically, biologically, and chemically. For all this aspect of quinone, Shahabadi *et al*. designed and synthesized a novel quinone derivative 40 (Figure 4) to investigate its binding interaction with BSA through spectrophotometry and spectrofluorimetry analysis [117]. Adding 40 to the buffer solution of BSA resulted in a static quenching in fluorescence at 346 nm.

On the other hand, adding 40 to the BSA also implied an increase in the absorption peak. The change in spectral behavior was observed due to the complexation between 40 and BSA with a binding constant of 3.2×104 M-1. The negative value of ΔG˚ and ΔH˚ and the positive value of ΔS˚ signified the formation of a stable BSA-40 complex through hydrophobic and hydrogen bonding interaction.

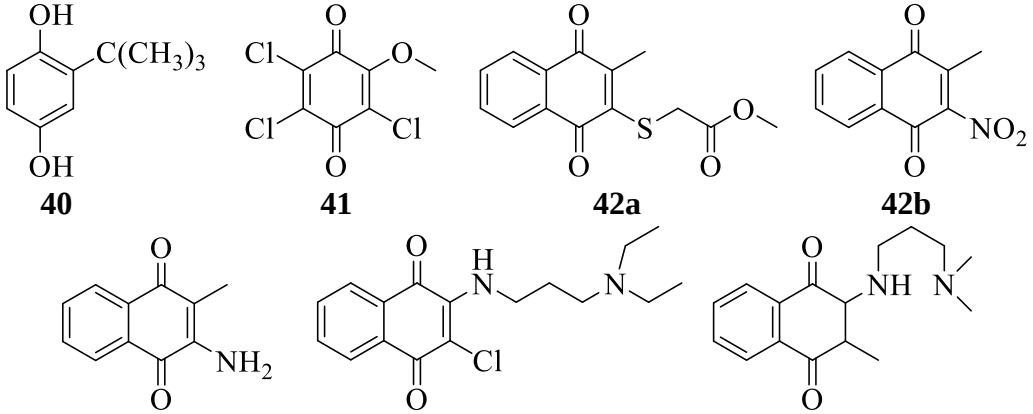

40 **41** **42a** **42b**

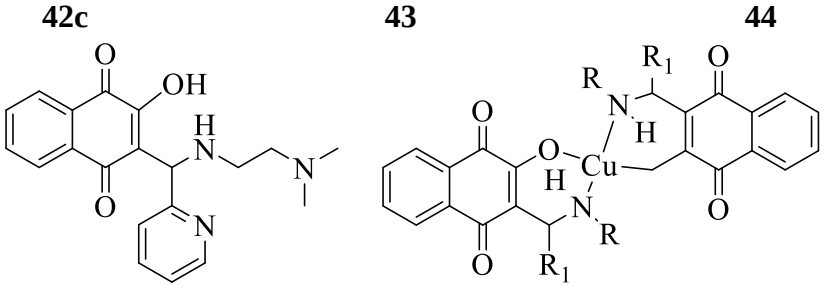

45 46a-e

46a: R = Nonane, R_1= 3-nitrotoluene
46b: R = Nonane, R_1= 2-hydroxy-5-methyl methoxy benzene
46c: R = Nonane, R_1= 3-bromotoluene
46d: R = Nonane, R_1= 1-methylpyridine
46e: R = But-1-ene, R_1= 2-hydroxy-5-methyl methoxy benzene

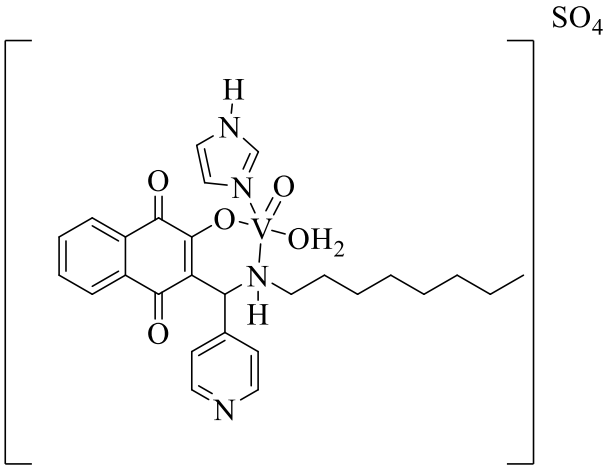

46f

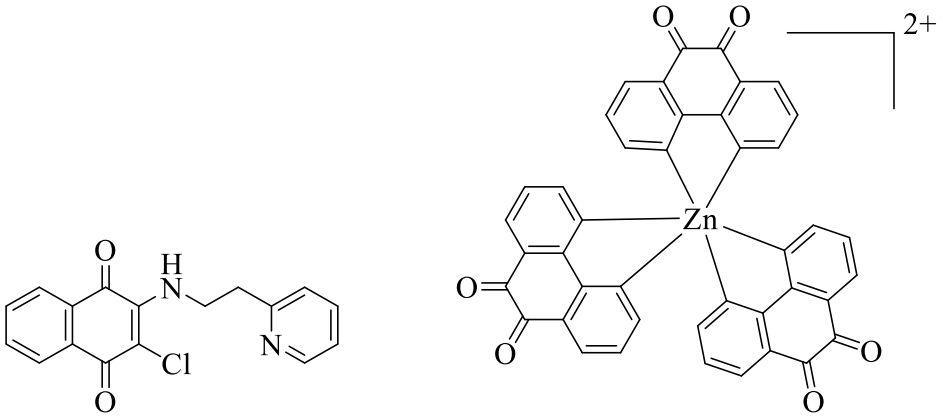

47 48

Figure 4. Quinone derivatives (40-48) as active binders of BSA.

A novel water-soluble quinone derivative 41 (Figure 4) was synthesized by Satheshkumar *et al*. to study its interaction with BSA through UV-visible and fluorescence spectra analysis [118]. Adding 41 to the buffer solution of BSA resulted in an alteration of the absorption band at 285 nm, 350 nm, and 534 nm with a distinct color change from yellow to pink. The fluorescence titration showed that the addition of 41 resulted in a quenching in fluorescence at 348 nm. The jobs plot data also confirmed that the complexation of 41 with BSA was a 1:1 stoichiometry ratio with a binding constant of 3.3×108 M-1. The BSA-41 complex can be utilized in various fields like pharmacy, pharmacology, and biochemistry. A series of vitamin K3 derivatives 42a-c (Figure 4) were synthesized by Suganthi *et al*. to

investigate their interaction with BSA in a phosphate buffer solution [119]. The quenched fluorescence of BSA in the presence of 42b signified the stable complex formation between 42b and BSA. The electron-withdrawing $–NO_2$ group in 42b influenced the hydrophobic interaction within the 42-BSA complex. The stability of the 42-BSA complex was also confirmed by thermodynamic parameters. The binding constant was calculated and found to be 4.6×105 M-1. The aminonapthoquinone-based ligand 43 (Figure 4) and its metal (II) complexes were devised by Kosiha *et al*. to investigate their binding interaction with BSA in Tris-HCl/NaCl buffer solution [120]. Upon the addition of 43 and its corresponding metal complexes to the BSA, the absorbance peak at 277 nm increases with a blue shift. The addition of 43 and its corresponding Co, Ni, Cu, and Zn metal complexes in the buffer decreased fluorescence intensity at 348 nm. The spectral analysis suggested the formation of a complex with BSA. The association constants of these BSA with 43 and their corresponding Cu, Co, Ni and Zn complexes were calculated and found to be 1.25×104, 2.39×105, 4.92×104, 1.79×104 and 4.92×104 M-1, respectively. The constant association value suggested the stable binding of metal complexes of 43 than 43 itself. The aminonapthoquinone-based ligand 44 (Figure 4) and its corresponding mononuclear metal (II) complexes of Co, Cu, and Zn were devised by Kosiha *et al*. to study their binding interaction with BSA by UV-vis and spectral fluorescence techniques [121]. The addition of 44 and its corresponding metal complex to the BSA in NaCl/Tris-HCl buffer displayed a gradual increase in the absorption band at 277 nm and quenching in fluorescence at 345 nm with a hypsochromic shift in fluorescence emission peak of BSA. The change in spectral behavior was due to the alteration of the microenvironment around the chromophore of the protein after complex formation. The binding constants of the 44 and its metal complexes of Co, Cu, and Zn with BSA were calculated and found to be 5.14×104, 5.76×105, 4.26×105 and 3.89×105 M-1, respectively. The metal complexes with BSA showed cytotoxicity against human breast and lung cancer. Suganthi *et al*. designed and synthesized a Mannich base of 2-hydroxy-1,4-napthoqinone 45 (Figure 4) and its corresponding Co, Ni, Cu, and Zn metal complexes to analyze its binding interaction with BSA [122]. The fluorescence titration showed that the addition of 45 and all of its metal complexes implied a quenching in the fluorescence of BSA with a slight blue shift of 1 to 4 nm. On the other hand, the addition of 45 and its corresponding metal complexes also resulted in a significant increase in the absorption peak of BSA at 277 nm. The value of thermodynamic parameters suggested the stable complex formation through hydrophobic interaction. The binding constants of 45 and its corresponding Co, Ni, Cu, and Zn metal complexes are calculated and found to be 3.4×105, 1.9×104, 7.5×105, 1.2×106 and 1.1×106 M-1, respectively. A series of copper complexes 46a-e (Figure 4) and vanadium complex 46f (Figure 4) of lawsone Mannich base were devised by Nariya *et al*. for its binding study with BSA [123]. The fluorescence titration revealed that adding all the metal complex 46a-f to BSA in buffer solution displayed a quenching in fluorescence at 346 nm. This quenching in fluorescence was observed due to static quenching. The spectroscopic analysis clearly indicated that the order of interaction of 46a-f with BSA was represented as 46e> 46d> 46f> 46a> 46c> 46b. The association constants were estimated and found to be 3.103 × 105, 2.4677 × 105, 1.43 × 105, 5.0384×106, 15.790×107 and 1.37×106 for 46a-f, respectively. The novel aminonapthoquinone-based ligand 47 (Figure 4) and its corresponding Co (II), Ni (II), Cu (II), and Zn (II) metal complexes have been synthesized by Koshika *et al*. to study its binding interaction with BSA [124]. The UV-vis titration result indicated that the absorption peak of BSA at 277 nm continuously increased in the presence of all the metal complexes of 47 due to

the conformational changes of the protein. On the other hand, adding metal complexes of 47 to BSA in the buffer displayed a quenched fluorescence with a slight blue shift. The quenching in fluorescence was due to the strong hydrophobic interaction between the BSA and metal complexes of 47 compounds. The binding constants were calculated and found to be 7.88×103, 2.20×104, 4.55×104, 3.29×104 and 5.89×104 M-1 for metal complexes of 47, respectively. Anjomshoa *et al*. reported a novel phendione-based Zn(II) nanocomplex 48 (Figure 4) to investigate its interaction with BSA in buffer [125]. The addition of 48 to BSA resulted in a quenching in fluorescence at 346 nm due to the conformational change of protein surface during 48-BSA complex formation. The negative value of ΔG° and positive values of ΔH° and ΔS° also suggested the stable complex formation of 48-BSA. The binding constant was estimated and found to be $1.4\times104\ M^{-1}$. These protein-coated 48 complexes were applied in the human carcinoma cell lines.

Table 4. Selective parameters of quinone derivatives as an active binder of BSA.

Receptor	Solvent	Binding Constant (M^{-1})	Mechanism	Application	Reference
40	Sodium phosphate buffer	3.2×10^4	Static Quenching	---	[117]
41	Phosphate buffer	3.3×10^8	Static Quenching	Pharmacy, pharmacology, and biochemistry	[118]
42	Phosphate buffer	4.6×10^5	Static Quenching (Hydrophobic interaction)	---	[119]
43	Tris-HCl/NaCl buffer	1.25×10^4 2.39×10^5 4.92×10^4 1.79×10^4 4.92×10^4	Static and dynamic Quenching	Cytotoxicity studies	[120]
44	Tris-HCl/NaCl buffer	5.14×10^4 5.76×10^5 4.26×10^5 3.89×10^5	Static Quenching	cytotoxicity against human breast and lung cancer	[121]
45	Phosphate buffer	3.4×10^5 1.9×10^4 7.5×10^5 1.2×10^6 1.1×10^6	Static Quenching (Hydrophobic interaction)	Biological activities	[122]
46	Tris- NaCl buffer	3.103×10^5, 2.4677×10^5, 1.43×10^5, 5.0384×10^6, 15.790×10^7 1.37×10^6	Static Quenching	Cytotoxicity studies	[123]
47	Phosphate buffer	7.88×10^3 2.20×10^4 4.55×10^4 3.29×10^4 5.89×10^4	Static Quenching (Hydrophobic interaction)	Cytotoxicity studies	[124]
48	Tris/NaCl buffer	1.4×10^4	Dynamic quenching	Cytotoxicity against the human carcinoma cell lines	[125]

2.5. Interaction of BSA with imidazolium salt.

Novel organic salts known as imidazolium salts are being used to analyze environmental sample data and are being evaluated as green chemicals for industrial volatile organic compounds [126-127]. Imidazolium salts have low melting temperatures below 100˚C. Due to their distinctive and appealing qualities, such as negligible vapor pressure, good

chemical or thermal stability, nonflammability, favorable conductivity, and low toxicity, imidazolium salts showed considerable promise as a potential replacement for conventional volatile organic solvents. They have been used in many different domains, such as electrochemistry, chemical sensors, synthesis, and separation [128-130]. So to further understand the structural and functional details of imidazolium salt type surfactant-protein interactions, it would be imperative to research the binding of imidazolium salts type surfactant to bovine serum albumin. On this note, the noble imidazolium containing amphiphiles of 1-(2-hydroxyethyl)alkylimidazolium bromide 49 (Figure 5) was designed and synthesized by Kuzentsova *et al*. to analyze its aggregation ability with BSA using tensiometry technique [131]. The tensiometry analysis showed that the aggregation capability of 49 was increased by 5 times after the addition of BSA. It confirmed the hydrophobic interaction between the lipophilic tails of 49 and the hydrophobic packet of the protein molecule. The fluorescence titration analysis also observed that the addition of different concentrations of 49 to BSA resulted in a decrease in emission peak at 349 nm. It suggested the strong binding interaction between 49 and BSA.

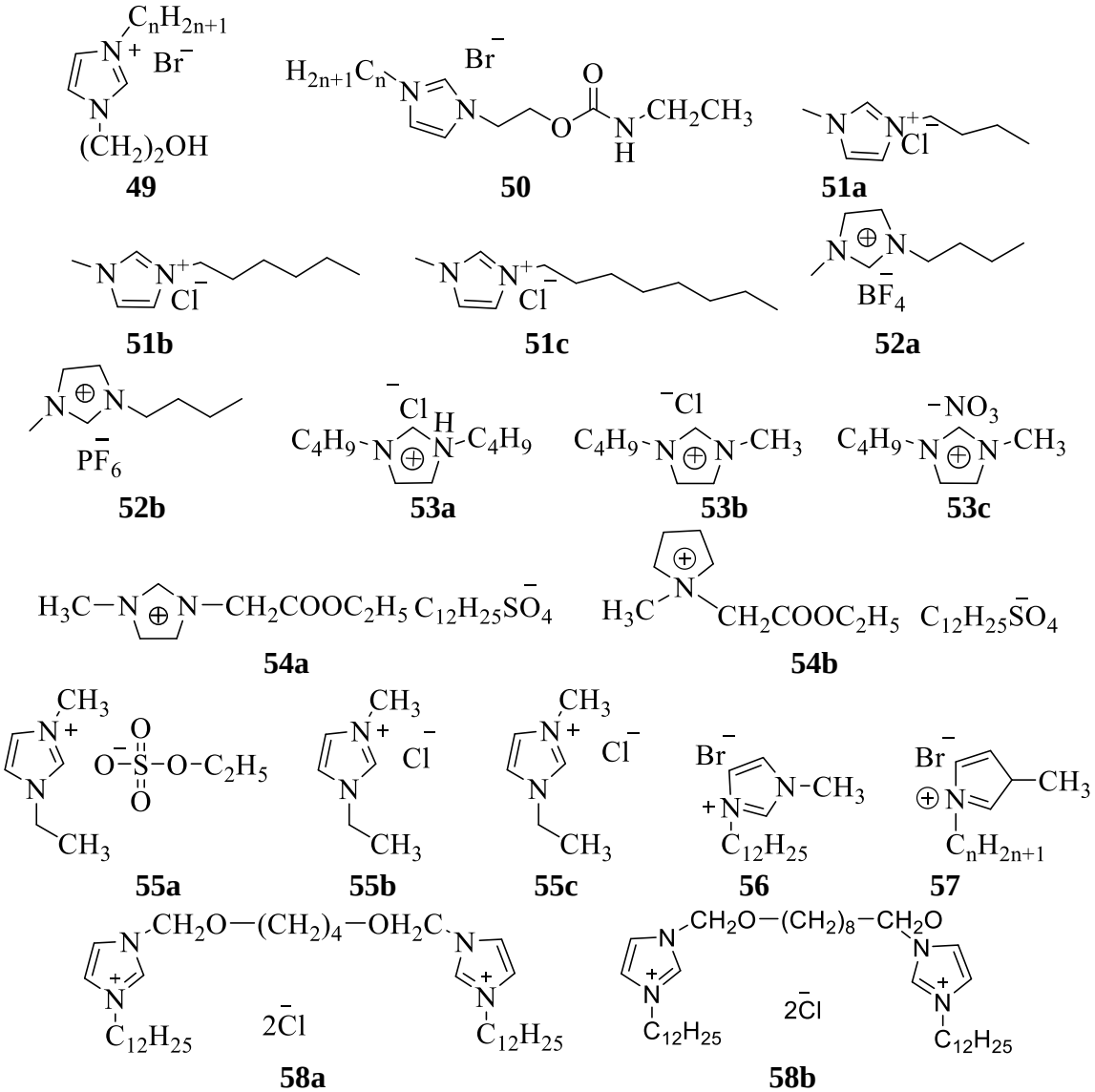

Figure 5. Imidazolium salts (49-58) as active binders of BSA.

Kuznetsova *et al*. reported amphiphiles bearing imidazolium and urethane moieties 50 (Figure 5) to analyze its complexation ability towards BSA through multi-physicochemical

methods [132]. The analysis revealed that the addition of 50 to BSA resulted in a decrease in the aggregation threshold of 50. Adding 50 to the buffer solution of BSA resulted in a quenching in fluorescence with a slight hypsochromic shift. The binding interaction depends upon the length of the tail of amphiphiles. The binding constant was calculated and found to be 0.26×104 M-1. The value of the thermodynamic parameter also suggested the formation of a stable complex. The binding interaction of a series of imidazolium chloride ionic liquids 51a-c (Figure 5) with BSA was studied by Huang *et al*. [133]. The investigation was performed through UV-vis and fluorescence spectral analysis. Adding 51a to BSA increased the absorption peak at 223 nm with a hypochromic shift from 223 nm to 237 nm. But adding 51b and 51c resulted in a decrease in absorption peak with a slight red shift. The addition of 51a-c also displayed a quenching fluorescence emission at 339 nm. The rate of the quenching effect depends upon the length of the hydrophobic carbon chain. The binding constants for 51a-c were calculated and found to be 0.16×102, 0.31×102, and 3.55×102 M-1, respectively. The interaction of BSA with synthesized alkyl imidazolium-based ionic liquids 52a and 52b (Figure 5) was studied by Zhu *et al*. through isothermal titration calorimetry (ITC) and circular dichroism (CD) [134]. CD spectrum showed that the interaction of 52a and 52b implied a slight decrease in band intensity of BSA at 208 and 222 nm. The change in spectral behavior was observed due to the change in the secondary structure of BSA. In ITC analysis, the degree of coincidence between the calculated curve and the experimental integrated heat suggested the existence of two types of active binding sites for 52a and 52b.

A series of imidazolium ionic liquids 53a-c (Figure 5) were reported by Shu *et al*. to investigate its binding interaction with BSA [135]. Due to complex dynamic collision, the addition of 53a-c to BSA in buffer solution resulted in a quenching in fluorescence at 340 nm. From the thermodynamic analysis, it was observed that the interaction between 53a and 53b was purely hydrophobic and electrostatic interaction. This kind of interaction caused the polypeptides in BSA to unfold. The molecular docking analysis confirmed the hydrophobic interaction between the cationic imidazolium moieties of 53a-c and the subdomain of the BSA cavity. The binding constants of 53a-c were evaluated and found to be 1.29×102, 1.06×102, and 5.19×102 M-1, respectively. Wang *et al*. reported two ester-functionalized anionic surface active ionic liquids 54a and 54b (Figure 5) to investigate their interaction with BSA in an aqueous solution through various techniques [136]. From the fluorescence titration analysis, it was observed that adding 54a and 54b to BSA resulted in a quenching in fluorescence at 348 nm with a clear blue shift. The change in spectral behavior was due to the hydrophobic interaction within the 54a-BSA and 54b-BSA complexes. The binding constants of complexes are calculated and found to be 3.092×103 and 1.689×103 M-1. The result showed that the cationic ring slightly affects the surface of the BSA. Satish *et al*. synthesized a series of imidazolium-based ionic liquids 55a-c (Figure 5) to investigate its interaction with BSA using different spectroscopic techniques [137]. Adding 55a-c to BSA in buffer solution resulted in a dynamic quenching in fluorescence. The thermodynamic analysis suggested the existence of weak interaction between BSA and 55a-c. The conformational change of BSA due to the formation of complexes was confirmed by CD analysis. The binding constants of 55a-c are calculated and found to be 3.43×104, 3.33×104, and 1.74×104 M-1, respectively. The aggregation ability of BSA with an imidazole-containing amphiphile system 56 (Figure 5) was studied by Samarkina *et al*. [138]. The surfactant 56 showed excellent binding interaction with BSA.

The addition of 56 to the BSA in the buffer solution implied a quenching in fluorescence at 348 nm with a clear blue shift. The size of the surfactant 56-BSA complexes was determined by dynamic light scattering to rely on the polypeptide size (6-10 nm) rather than the concentrations of the surfactant and BSA. Tensiometry analysis revealed that the system's aggregation threshold is reduced by a factor of 50 when BSA is added to the surfactant. The binding constant of the 56-BSA complex was evaluated and found to be 0.58×103 M-1. Using various physiochemical methods, the binding interaction of a series of amphiphiles bearing imidazole 57 (Figure 5) with BSA was investigated by Samarkina *et al*. [139]. The addition of 57 resulted in a quenching in the fluorescence of BSA at 285 nm. The dynamic light scattering research revealed that the size of the surfactant 57–BSA complex is governed by the polypeptide size and is constant over the whole amphiphile concentration range.

Additionally, it has been demonstrated that adding BSA to the surfactant solution of 57 leads to a 45-fold reduction in aggregation threshold. The binding constant was calculated and found to be 7.07×102 M-1. The interaction of two imidazolium-derived gemini surfactants 58a and 58b (Figure 5) with BSA was analyzed by Gospodarczyk *et al*. through circular dichroism (CD) analysis [140]. From the CD analysis, a significant change in the protein's radius of gyration and a significant alteration of the secondary structure of BSA in the presence of 58a and 58b was observed. It was also observed that the radius of gyration increased dramatically with the addition of surfactants 58a and 58b and decreased with high surfactant concentrations. BSA has also been seen to aggregate strongly for a specific range of surfactant concentrations.

Table 5. Selective parameters of various imidazolium salts as an active binder of BSA.

Receptor	Solvent	Binding Constant (M^{-1})	Mechanism	Application	References
49	Phosphate buffer	---	Static quenching (Hydrophobic Interaction)	Pharmaceutical application	[131]
50	Phosphate buffer	0.26×10^{4}	Static quenching	---	[132]
51	Tris/NaCl buffer	0.16×10^{2} 0.31×10^{2} 3.55×10^{2}	Static quenching	Biomedical application	[133]
52	Phosphate buffer	---	Hydrophobic Interaction	Biochemical analysis	[134]
53	Tris-HCl buffer	1.29×10^{2} 1.06×10^{2} 5.19×10^{2}	Static and dynamic quenching	---	[135]
54	Phosphate buffer	3.092×10^{3} 1.689×10^{3}	Static quenching (Hydrophobic Interaction)	Surface water analysis	[136]
55	Phosphate buffer	3.43×10^{4} 3.33×10^{4} 1.74×10^{4}	Dynamic quenching	---	[137]
56	Phosphate buffer	0.58×10^{3}	Static and dynamic quenching	Biomedical application	[138]
57	Phosphate buffer	7.07×10^{2}	Dynamic quenching	Pharmaceutical application	[139]
58	Tris-HCl buffer	---	Static quenching (Hydrophobic Interaction)	Surface water analysis	[140]

3. Conclusions

Interactions between various molecular probes and BSA are one of the promising types of molecules showing antibacterial, antiviral, anticancer, antioxidant, and antineoplastic

potential in the context of the increasing incidence of drug resistance. Studying and comprehending a drug's capacity to bind to albumin is one of the vital phases in creating a novel and efficient drug, as they are essential to its transport, metabolism, distribution, and excretion. In light of this, we emphasized the key ideas regarding the structure and roles of bovine serum albumin (BSA) and the factors to be considered while designing coordination complexes with protein binding capacities. In addition, the most crucial instrumentation methods used to investigate the nature and strength of the coordinated complex-BSA interactions are fluorescence spectroscopy, UV-Vis absorption spectroscopy, circular dichroism study, and molecular docking study.

Funding

Dr. Jali acknowledges a fund from DST-Biotechnology, Govt. of Odisha, and Project No.: ST-BT-MISC-0008-2020-245/ST, dated 12-01-2022.

Acknowledgments

The authors also thank the Department of Chemistry, VSSUT, Burla, for providing a research facility.

Conflicts of Interest

The authors declare that they have no known competing financial interests or personal relationships that could have appeared to influence the work reported in this paper.

References:

1. Ogbodu, R. O.; Nyokong, T. Effects of number of ring substituents on the physicochemical properties of zinc aminophenoxy phthalocyanine-single walled carbon nanotube conjugate. *J. Photochem. Photobiol* **2014**, *274*, 83-90, https://doi.org/10.1016/j.jphotochem.2013.09.015.
2. Behera, S.; Behura, R.; Mohanty, M.; Dinda, R.; Mohanty, P.; Verma, A. K.; Sahoo, S. K.; Jali, B. R. Spectroscopic, cytotoxicity and molecular docking studies on the interaction between 2, 4-dinitrophenylhydrazine derived Schiff bases with bovine serum albumin. *Sensors International* **2020,** *1*, 100048, https://doi.org/10.1016/j.sintl.2020.100048.
3. Naveenraj, S.; Asiri, A. M.; Anandan, S. Interaction between serum albumins and sonochemically synthesized cadmium sulphide nanoparticles: a spectroscopic study. *J. Nanoparticle Res* **2013**, *15*, 1-12, https://doi.org/10.1007/s11051-013-1671-9.
4. Peters, T. J. All about albumin. *Academic Press*. **1996**, https://www.sciencedirect.com/book/9780125521109/all-about-albumin.
5. Carter, D. C.; Ho, J. X. Structure of serum albumin, *Adv. Protein Chem. Struct. Biol* **1994**, *45*, 153, https://doi.org/10.1016/S0065-3233(08)60640-3 .
6. Behera, S.; Behura, R.; Mohanty, P.; Sahoo, M.; Duggirala, R. Study of interaction between bovine serum albumin and dolutegravir intermediate: Fluorescence and molecular docking Analysis. *Biointerface Res. Appl. Chem* **2021**, *11*, 13102-13110, https://doi.org/10.33263/BRIAC115.1310213110.
7. Peters, T. J. Metabolism: albumin in the body, All about albumin, Biochemistry Genetics and Medical applications. *San Diego: Academic Press*. **1996**, *188*, https://www.elsevier.com/books/all-about-albumin/peters-jr/978-0-12-552110-9.
8. Pappen, F. G.; Qian, W.; Aleksejūnienė, J.; Leonardo, R. de-Toledo.; Leonardo, M. R.; Haapasalo, M. Inhibition of sodium hypochlorite antimicrobial activity in the presence of bovine serum albumin, *J. Endod* **2010,** *36*, 268-271, https://doi.org/10.1016/j.joen.2009.09.025.
9. Khan, Z.; Al-Thabaiti, S. A. Green synthesis of zero-valent Fe-nanoparticles: catalytic degradation of rhodamine B, interactions with bovine serum albumin and their enhanced antimicrobial activities, *J. Photochem. Photobiol. B, Biol* **2018,** *180*, 259-267, https://doi.org/10.1016/j.jphotobiol.2018.02.017.

10. Espinosa-Cristóbal, L. F.; Martínez-Castañón, G. A.; Loyola-Rodríguez, J. P.; Niño-Martínez, N.; Ruiz, F.; Zavala-Alonso, N. V.; Lara, R. H.; Reyes-López, S. Y. Bovine serum albumin and chitosan coated silver nanoparticles and its antimicrobial activity against oral and nonoral bacteria. *J. Nanomater* **2015**, https://doi.org/10.1155/2015/420853
11. Rani, J. J.; Jayaseeli, A. M. I.; Sankarganesh, M.; Asha, R. N. Bovine serum albumin interaction, molecular docking, anticancer and antimicrobial activities of Co (II) Schiff base complex derived from Nophen ligand. *J. Biomol. Struct. Dyn* **2022**, 1-9, https://doi.org/10.1080/07391102.2022.2026249.
12. Sahoo, P. M. S.; Behera, S.; Behura, R.; Acharya, A.; Biswal, D.; Suna, S. K.; Sahoo, R.; Soren, R. C.; Jali, B. R. A brief review: Antibacterial activity of Quinone derivatives. *Biointerface Res. Appl. Chem* **2022,** *12*, 3247-3258, https://doi.org/10.33263/ BRIAC123.32473258.
13. Mohanty, P.; Behera, S.; Behura, R.; Shubhadarshinee, L.; Mohapatra, P.; Barick, A. K.; Jali, B. R. Antibacterial Activity of Thiazole and its Derivatives: A. *Biointerface Res. Appl. Chem* **2021**, https://doi.org/10.33263/BRIAC122.21712195.
14. Behera, S.; Mohanty, P.; Behura, R.; Nath, B.; Barick, A. K.; Jali, B. R. Antibacterial properties of quinoline derivatives: A Mini**.** *Biointerface Res. Appl. Chem* **2021**, https://doi.org/10.33263/BRIAC125.60786092.
15. Guo, L.; Peng, Y.; Yao, J.; Sui, L.; Gu, A.; Wang, J. Anticancer activity and molecular mechanism of resveratrol–Bovine serum albumin nanoparticles on subcutaneously implanted human primary ovarian carcinoma cells in Nude mice. *Cancer Biother. Radiopharm* **2010**, *25*, 471-477, https://doi.org/10.1089/cbr.2009.0724.
16. Naso, L.; Martínez, V. R.; Lezama, L.; Salado, C.; Valcarcel, M.; Ferrer, E. G.; Williams, P. A. Antioxidant, anticancer activities and mechanistic studies of the flavone glycoside diosmin and its oxidovanadium (IV) complex. Interactions with bovine serum albumin. *Bioorg. Med. Chem* **2016**, *24*, 4108-4119, https://doi.org/10.1016/j.bmc.2016.06.053.
17. Rani, J. J.; Jayaseeli, A. M. I.; Sankarganesh, M.; Asha, R. N. Bovine serum albumin interaction, molecular docking, anticancer and antimicrobial activities of Co (II) Schiff base complex derived from Nophen ligand. *J. Biomol. Struct. Dyn* **2022**, 1-9, https://doi.org/10.1080/07391102.2022.2026249.
18. Jali, B. R.; Kuang, Y.; Neamati, N.; Baruah. J. B. Selective binding of naphthoquinone derivatives to serum albumin proteins and their effects on cytotoxicity. *Chem.-Biol. Interact* **2014,** *214*, 10-17, https://doi.org/10.1016/j.cbi.2014.01.014.
19. Zang, Z.; Chou, S.; Si, X.; Cui, H.; Tan, H.; Ding, Y.; Liu, Z.; Wang, H.; Lang, Y.; Tang, S.; Li, B. Effect of bovine serum albumin on the stability and antioxidant activity of blueberry anthocyanins during processing and *in vitro* simulated digestion, *Food Chem* **2022**, *373*, 131496, https://doi.org/10.1016/j.foodchem.2021.131496.
20. Al-Rahim, A. M.; Mahmood, R. I.; Mohammed, M. M.; Omer, D. *In vitro* evaluation of antioxidant and cytotoxic activity of folate-methotrexate conjugated to bovine serum albumin nanoparticles against MCF-7, HepG2, and PC3 cell lines, *Gene Rep* **2022**, *29*, 101666, https://doi.org/10.1016/j.genrep.2022.101666.
21. Fan, Y.; Yi, J.; Zhang, Y.; Yokoyama, W. Fabrication of curcumin-loaded bovine serum albumin (BSA)-dextran nanoparticles and the cellular antioxidant activity. *Food Chem* **2018,** *239*, 1210-1218, https://doi.org/10.1016/j.foodchem.2017.07.075.
22. Fonseca, D. P.; Khalil, N. M.; Mainardes, R. M. Bovine serum albumin-based nanoparticles containing resveratrol: Characterization and antioxidant activity. *J. Drug. Deliv. Sci. Technol* **2017**, *39*, 147, https://doi.org/10.1016/j.foodchem.2017.07.075.
23. Xiao, J.; Suzuki, M.; Jiang, X.; Chen, X.; Yamamoto, K.; Ren, F.; Xu, M. Influence of B-ring hydroxylation on interactions of flavonols with bovine serum albumin. *J. Agric. Food Chem* **2008**, *56*, 2350-2356, https://doi.org/10.1021/jf7037295.
24. Antçnio, E.; Khalil, N. M.; Mainardes, R. M. Bovine serum albumin nanoparticles containing quercetin: characterization and antioxidant activity. *J. Nanosci. Nanotechnol* **2016**, *16*, 1346-1353, https://doi.org/10.1166/jnn.2016.11672.
25. Sandu, N.; Chilom, C. G.; Florescu, M. Molecular insights into binding mechanism of rutin to bovine serum albumin–Levothyroxine complex: Spectroscopic and molecular docking approaches, *Spectrochim. Acta A Mol. Biomol. Spectrosc* **2022**, *264*, 120261, https://doi.org/10.1016/j.saa.2021.120261.
26. He, X. M.; Carter, D. C. Atomic structure and chemistry of human serum albumin. *Nature* **1992**, *358*, 209, https://doi.org/10.1038/358209a0.
27. Brown, J. R. Serum albumin: amino acid sequence in Albumin: Structure, Function and Uses. *Pergamon* **1977**, *27-52b*, https://doi.org/10.1016/B978-0-08-019603-9.50009-0.

28. Weijers, R. N. Amino acid sequence in bovine serum albumin. *Clin. Chem* **1977**, *23*, 1361-1362, https://www.researchgate.net/profile/Rob-Weijers/publication/22283331_Amino_acid_sequence_in_bovine_serum_albumin/links/09e4150c0686fad851000000/Amino-acid-sequence-in-bovine-serum-albumin.pdf.
29. Zapun, A.; Bardwell, J. C.; Creighton, T. E. The reactive and destabilizing disulphide bond of DsbA, a protein required for protein disulphide bond formation *in vivo*. *Biochem* **1993**, *32*, 5083-5092, https://doi.org/10.1021/bi00070a016.
30. Dill, K. A.; Shortle, D. Denatured states of proteins. *Annu. Rev. Biochem* **1991**, *60*, 795-825, https://www.annualreviews.org/doi/abs/10.1146/annurev.bi.60.070191.004051?journalCode=biochem.
31. Dobson, C. M.; Principles of protein folding, misfolding and aggregation, Semin. *Cell Dev. Biol* **2004**, *15*, 1, 3-16, https://doi.org/10.1016/j.semcdb.2003.12.008.
32. Mohanty, P.; Behura, R.; Bhardwaj, V.; Dash, P. P.; Sahoo, S. K.; Jali, B. R. Recent advancement on chromo-fluorogenic sensing of aluminum (III) with Schiff bases. *Trends Environ. Anal. Chem* **2022**, 00166, https://doi.org/10.1016/j.teac.2022.e00166.
33. Behura, R.; Behera, S.; Mohanty, P.; Dash, P. P.; Panigrahi, R.; Mallik, B. S.; Sahoo, S. K.; Jali, B. R. Fluorescent sensing of water in DMSO by 2, 4-dinitrophenyl hydrazine derived Schiff base. *J. Mol. Struct* **2022**, *1251*, 132086. https://doi.org/10.1016/j.molstruc.2021.132086.
34. Jali, B. R.; Thakur, S. R.; Behura, R.; Behera, S.; Sayala, R. B.; Barick, A. K. Selective detection of fluoride and hydrogen sulfate anions by pyrimidine-based fluorescence chemosensor. *Indian J. Chem. A* **2020**, *59(12)*, 1809-1813, https://doi.org/10.56042/ijca.v59i12.29642.
35. Rashtbari, S.; Dehghan, G.; Sadeghi, L.; Sareminia, L.; Iranshahy, M.; Iranshahi, M.; Khataee, A.; Yoon, Y. Interaction of bovine serum albumin with ellagic acid and urolithins A and B: Insights from surface plasmon resonance, fluorescence, and molecular docking techniques. *Food Chem. Toxicol* **2022,** *162*, 112913, https://doi.org/10.1016/j.fct.2022.112913 .
36. Jali, B. R.; Behura, R.; Barik, S. R.; Parveen, S.; Mohanty, S. P.; Das, R. A brief review: biological implications of naphthoquinone derivatives. *Res J Pharm Technol* **2018**, *11*, 3698-3702, https://doi.org/10.5958/0974-360X.2018.00679.0.
37. Geng, Y.; Zhang, S.; Wang, Y.; Ye, N.; Xiang, Y. Aptamer act as fluorescence switching of bovine serum albumin stabilized gold nanoclusters for ultrasensitive detection of kanamycin in milk. *Microchem. J* **2021,** *165*, 106145, https://doi.org/10.1016/j.microc.2021.106145.
38. Jali, B. R.; Baruah, J. B. Recent progress in Schiff bases in detections of fluoride ions. *Dyes Pigm* **2021**, *194*, 109575, https://doi.org/10.1016/j.dyepig.2021.109575.
39. Sułkowska, A.; Równicka, J.; Pożycka, J.; Bojko, B.; Sułkowski, W. W. The effect of concentration of guanidine hydrochloride on the sulfasalazine–serum albumin complex. *J. Mol. Struct*, **2005,** *744*, 775-779, https://doi.org/10.1016/j.molstruc.2004.10.093.
40. Liu, S.; Wang, S. E.; Liu, Z.; Investigating the size-dependent binding of pristine nC60 to bovine serum albumin by multi-spectroscopic techniques. *Materials*, **2021**, *14*, 298, https://doi.org/10.3390/ma14020298 .
41. Zhang, Y. Z.; Zhou, B.; Liu, Y. X.; Zhou, C. X.; Ding, X. L.; Liu, Y. Fluorescence study on the interaction of bovine serum albumin with p-aminoazobenzene. *J. Fluoresc* **2008**, *18*, 109-118, https://doi.org/10.1007/s10895-007-0247-4.
42. Hu, Y. J.; Liu, Y.; Zhang, L. X.; Zhao, R. M.; Qu, S. S. Studies of interaction between colchicine and bovine serum albumin by fluorescence quenching method. *J. Mol. Struct* **2005**, *750*, 174-178, https://doi.org/10.1016/j.molstruc.2005.04.032.
43. Nan, Z.; Hao, C.; Ye, X.; Feng, Y.; Sun, R. Interaction of graphene oxide with bovine serum albumin: A fluoescence quenching study. *Spectrochim. Acta - A: Mol. Biomol* **2019**, *210*, 348-354, https://doi.org/10.1016/j.saa.2018.11.028.
44. Zhang, J.; Yan, Q.; Liu, J.; Lu, X.; Zhu, Y.; Wang, J.; Wang, S. Study of the interaction between 5-sulfosalicylic acid and bovine serum albumin by fluorescence spectroscopy. *J. Lumin* **2013**, *134*, 747-753, https://doi.org/10.1016/j.jlumin.2012.06.053.
45. Puchtler, H.; Meloan, S. On Schiff's bases and aldehyde-Fuchsin: a review from H. Schiff to R. D. Lillie. *Histochemistry*, **1981,** *72*, 321-332. https://doi.org/10.1007/BF00501774.
46. Kashanian, S.; Gholivand, M. B.; Ahmadia, F.; Taravati, A.; Colagar, A. H. DNA interaction with Al-N,N'bis (salicylidene) 2,2'-phenylendiamine complex. *Spectrochim. Acta A* **2007**, *67*,472-478, https://doi.org/10.1016/j.saa.2006.08.017.

47. Patel N. B.; Patel, V. N. Synthesis and antimicrobial evaluation of w(4-Oxo-thiazolidinyl) quinazolin – 4(3H) ones o [(2,6-Dichlorophenyl)amino] phenylacetic acid. *Iran. J. Pharm. Res* **2007**, *6*, 251-258, https://dx.doi.org/10.22037/ijpr.2010.729.
48. Kumar, K. S.; Ganguly, S.; Veerasamy. R.; Clercq, E. D. Synthesis, antiviral activity and cytotoxicity evaluation of Schiff bases of some 2-phenyl quinazoline-4 (3) H-ones. *Eur. J. Med. Chem* **2010**, *45*, 5474, https://doi.org/10.1016/j.ejmech.2010.07.058.
49. Tangestaninejad, S.; Moghadam, M.; Mirkhani, V.; Mohammadpoor-Baltork, I.; Ghani, K. Alkene epoxidation catalysed by molybdenum supported on functionalized MCM-41 containing N-S chelating Schiff base ligand. *Catal. Commun* **2009,** *10*, 853-858, https://doi.org/10.1016/j.catcom.2008.12.010.
50. Berhanu, A. L.; Mohiuddin, I.; Malik, A. K.; Aulakh, J. S.; Kumar, V.; Kim, K. H. A review of the applications of Schiff bases as optical chemical sensors. *Trends. Analyt. Chem* **2019**, *116*, 74-91, https://doi.org/10.1016/j.trac.2019.04.025.
51. Jia, Y.; Li, J. Molecular assembly of Schiff base interactions: Construction and application. *Chem. Rev* **2015**, *115*, 1597-1621, https://doi.org/10.1021/cr400559g.
52. Kumbar, N. S. S.; Hosamani, K. M.; Gouripur, G. C.; Joshi, S. D. Functionalization of 3 chloroformyl coumarin to coumarin Schiff bases using reusable catalyst: an approach to molecular docking and biological studies. *R. Soc. open sci* **2018**, *5*, 172416, https://doi.org/10.1098/rsos.172416.
53. Li, L.; Li, Z.; Wang, K.; Zhao, S.; Feng, J.; Li, J.; Yang, P.; Liu, Y.; Wang, L.; Li, Y.; Shang, H.; Wang, Q. Design, synthesis, and biological activities of aromatic gossypol Schiff base derivatives. *J. Agric. Food Chem* **2014**, *62*, 11080-11088, https://doi.org/10.1021/jf504411g.
54. Hameed, A.; Al-Rashida, M.; Uroos, M.; Ali, S. A.; Khan, K. M. Schiff bases in medicinal chemistry: a patent review (2010-2015). *Expert Opin. Ther. Pat* **2017**, *27*, 63-79, https://doi.org/10.1080/13543776.2017.1252752.
55. Haj, N. Q.; Mohammed, M. O.; Mohammood, L. E. Synthesis and Biological evaluation of three new chitosan Schiff base derivatives. *ACS Omega* **2020**, *5* , 13948-13954, https://doi.org/10.1021/acsomega.0c01342.
56. Kirar, J. S.; Khare, S. Cu (II) Schiff base complex intercalated into layered double hydroxide for selective oxidation of ethyl benzene under solvent-free conditions. *RSC Adv.* **2018**, *8*, 18814, https://doi.org/10.1021/acsomega.0c01342.
57. Carreno, A.; Zuniga, C.; Hernandez, D. P.; Gacitua, M.; Polanco, R.; Otero, C.; Perez, R. A.; Fuentes, J. A. Study of structure-bioactivity relationship of three new pyridine Schiff bases: Synthesis, spectral characterization, DFT calculations and biological assays. *New J. Chem* **2018**, *42*, 8851-8863, https://doi.org/10.1039/C8NJ00390D.
58. Ping, M.; Yang, L.; Yezhong, Z.; Jiaxin, F.; Xiaohong, S.; Yi, L. Binding Studies of a Schiff Base Compound Containing a 1, 2, 4-Triazole Ring with Bovine Serum Albumin Using Spectroscopic Methods. *Chinese J. Chem* **2010**, *28*, 1915-1922, https://doi.org/10.1002/cjoc.201090319.
59. Padalkar, V. S.; Patil, V. S.; Telore, R. D.; Sekar, N. Synthesis of novel fluorescent 1, 3, 5-trisubstituted triazine derivatives and photophysical property evaluation of fluorophores and their BSA conjugates. *Heterocycl. Comm **2012**, 18*, 127-134, https://doi.org/10.1515/hc-2012-0024.
60. Andrezálová, L.; Plšíková, J.; Janočková, J.; Koňariková, K.; Žitňanová, I.; Kohútová, M.; Kožurková, M. DNA/BSA binding ability and genotoxic effect of mono-and binuclear copper (II) complexes containing a Schiff base derived from salicylaldehyde and D, L-glutamic acid. *J. Organomet. Chem* **2017**, *827*, 67-77, https://doi.org/10.1016/j.jorganchem.2016.11.007.
61. Bozkurt, E.; Gul, H. I. Deciphering binding mechanism between bovine serum albumin and new pyrazoline compound. *J. Lumin* **2020**, *35*, 534-541. https://doi.org/10.1002/bio.3762.
62. Liu, B. M.; Ma, P.; Wang, X.; Kong, Y. M.; Zhang, L. P.; Liu, B. Synthesis of three rimantadine Schiff Bases and their biological effects on serum albumin. *Iran. J. Pharm. Res* **2014,** *13*, 1183-1190, https://pubmed.ncbi.nlm.nih.gov/25587306/.
63. Densil, S.; Chang, C. H.; Chen, C. L.; Mathavan, A.; Ramdass, A.; Sathish, V.; Thanasekaran, P.; Li, W. S.; Rajagopal, S. Aggregation-induced emission enhancement of anthracene-derived Schiff base compounds and their application as a sensor for bovine serum albumin and optical cell imaging. *J. Lumin* **2018**, *33* ,780-789, https://doi.org/10.1002/bio.3477.
64. Prashanth, M. K.; Madaiah, M.; Revanasiddappa, H. D.; Amruthesh, K. N. Synthesis, characterization, and BSA binding studies of some new benzamides related to Schiff base. *Int. sch. res. Notices* **2013**, https://doi.org/10.1155/2013/791591.

65. Srinivasan, V.; Khamrang, T.; Ponraj, C.; Saravanan, D.; Yamini, R.; Beraand S.; Jhonsi, M. A. Pyrene based Schiff bases: Synthesis, crystal structure, antibacterial and BSA binding studies. *J. Mol. Struct* **2021**, *1225*, 129153, https://doi.org/10.1016/j.molstruc.2020.129153.
66. Sengottiyan, S.; Malakar, K.; Kathiravan, A.; Velusamy, M.; Mikolajczyk, A.; Puzyn, T. Integrated approach to interaction studies of pyrene derivatives with bovine serum albumin: insights from theory and experiment. *J. Phys. Chem. B* **2022**, *126*, 3831-3843, https://doi.org/10.1021/acs.jpcb.2c00778.
67. Niu, H. Y.; Liu, B.; Ma, P.; Wang, X.; Liu, B. M.; Wang, D. J. Study of the Interaction between three new Amantadine Schiff Bases and BSA by the Multi-spectroscopic Method. *Appl. Mech. Mater* **2013**, *239*, 193, https://doi.org/10.4028/www.scientific.net/AMM.239-240.193.
68. Gurusamy, S.; Krishnaveni, K.; Sankarganesh, M.; Asha, R. N.; Mathavan, A. Synthesis, characterization, DNA interaction, BSA/HSA binding activities of VO (IV), Cu (II) and Zn (II) Schiff base complexes and its molecular docking with biomolecules. *J. Mol. Liq* **2022**, *345*, 117045, https://doi.org/10.1016/j.molliq.2021.117045.
69. Sathyadevi, P.; Krishnamoorthy, P.; Butorac, R. R.; Cowley, A. H.; Bhuvaneshand, N. S.; Dharmaraj, N. Effect of substitution and planarity of the ligand on DNA/BSA interaction, free radical scavenging and cytotoxicity of diamagnetic Ni (II) complexes: a systematic investigation. *Dalton Trans **2011**, 40*, 9690-9702, https://doi.org/10.1039/C1DT10767D.
70. Balakrishnan, N.; Haribabu, J.; Krishnan, D. A.; Swaminathan, S.; Mahendiran, D.; Bhuvanesh, N. S.; Karvembu, R. Zinc (II) complexes of indole thiosemicarbazones: DNA/protein binding, molecular docking and *in vitro* cytotoxicity studies. *Polyhedron* **2019**, *170*, 188-201, https://doi.org/10.1016/j.poly.2019.05.039.
71. Dezhampanah, H.; Firouzi, R.; Shoeili, Z. M.; Binazir, R. Intermolecular investigation on interaction of two ternary copper (II) Schiff base complexes with bovine serum albumin. *J. Mol. Struc* **2020**, *1205*, 127557, https://doi.org/10.1016/j.molstruc.2019.127557.
72. Keshavarzian, E.; Asadi, Z.; Kucerakova, M.; Dusek, M.; Rastegari, B. DNA interaction and BSA binding of O-vanillin-based new Schiff base Co (III) and Ni (II) complexes: Theoretical, experimental, antibacterial and anticancer studies. *Polyhedron* **2022**, *223*, *2*115987, https://doi.org/10.1016/j.poly.2022.115987.
73. Li, L.; Guo, Q.; Dong, J.; Xu, T.; Li, J. DNA binding, DNA cleavage and BSA interaction of a mixed-ligand copper (II) complex with taurine Schiff base and 1, 10-phenanthroline. *J. Photochem. Photobiol. B* **2013**, *125*, 56-62, https://doi.org/10.1016/j.jphotobiol.2013.05.007.
74. Mallick, A.; Bera, S. C.; Maiti, S.; Chattopadhyay, N. Fluorometric investigation of interaction of 3-acetyl-4-oxo-6, 7-dihydro-12H indolo-[2, 3-a] quinolizine with bovine serum albumin. *Biophys. Chem.* **2004**, *112*, 9-14, https://doi.org/10.1016/j.bpc.2004.06.009.
75. Kandagal, P. B.; Ashoka, S.; Shaikh, S. M. Study of the interaction of an anticancer drug with human and bovine serum albumin: spectroscopic approach. *J. Pharm. Biomed. Anal* **2006**, *41*, 393-399, https://doi.org/10.1016/j.jpba.2005.11.037.
76. Silva, D.; Cortez, C. M.; Cunha-Bastos, J.; Louro, S. R. W. Methyl parathion interaction with human and bovine serum albumin. *Toxicol. Lett* **2004**, *147*, 53-61, https://doi.org/10.1016/j.toxlet.2003.10.014.
77. Zhang, Y. F.; Zhou, K. L.; Lou, Y. Y.; Pan, D. Q.; Shi, J. H. Investigation of the binding interaction between estazolam and bovine serum albumin: multi-spectroscopic methods and molecular docking technique. *J. Biomol. Struct. Dyn* **2017**, *35*, 3605-3614, https://doi.org/10.1080/07391102.2016.1264889.
78. Sun, X.; Bi, S.; Wu, J.; Zhao, R.; Shao, D.; Song, Z. Multispectral and molecular docking investigations on the interaction of primethamine/trimethoprim with BSA/HSA. *J. Biomol. Struct. Dyn* **2020**, *38*, 934-942, https://doi.org/10.1080/07391102.2019.1588785.
79. Khatun, S.; Yasmeen, S.; Kumar, A.; Subbarao, N. Calorimetric, spectroscopic and molecular modelling insight into the interaction of gallic acid with bovine serum albumin. *J. Chem. Thermodyn* **2018,** *122*, 85-94, https://doi.org/10.1016/j.jct.2018.03.004.
80. Shiraz, Z. A.; Sohrabi, N.; Moghadam, M. E.; Oftadeh, M. Dynamic and thermodynamic investigation on the interaction of bovine serum albumin with an anticancer Pt complex containing dithiocarbamate using molecular docking and spectroscopic methods. *Polycycl. Aromat. Compd* **2022**, 1-21, https://doi.org/10.1080/10406638.2022.2058027.
81. Nafisi, S.; Sadeghi, G. B.; PanahYab, A. Interaction of aspirin and vitamin C with bovine serum albumin. *J. Photochem. Photobiol. B, Biol* **2011,** *105(3)*, 198-202, https://doi.org/10.1016/j.jphotobiol.2011.09.002.
82. Wani, T. A.; Bakheit, A. H.; Abounassif, M. A.; Zargar, S. Study of interactions of an anticancer drug neratinib with bovine serum albumin: spectroscopic and molecular docking approach. *Front. Chem*, **2018**, *6*, 47, https://doi.org/10.3389/fchem.2018.00047.

83. Chaves, O. A.; da Silva, V. A.; Sant'Anna, C. M. R.; Ferreira, A. B.; Ribeiro, T. A. N.; de-Carvalho, M. G.; Cesarin-Sobrinho, D.; Netto-Ferreira, J. C. Binding studies of lophirone B with bovine serum albumin (BSA): Combination of spectroscopic and molecular docking techniques. *J. Mol. Struct* **2017**, *1128*, 606, https://doi.org/10.1016/j.molstruc.2016.09.036.
84. Patel, R.; Singh, B.; Sharma, A.; Saraswat, J.; Dohare, N.; ud-din Parray, M.; Siddiquee, M. A.; Alanazi, A. M.; Khan, A. A. Interaction and esterase activity of albumin serums with orphenadrine: A spectroscopic and computational approach. *J. Mol. Struct* **2021**, *1239*, 130522, https://doi.org/10.1016/j.molstruc.2021.130522.
85. Tian, Z.; Zang, F.; Luo, W.; Zhao, Z.; Wang, Y.; Xu, X.; Wang, C. Spectroscopic study on the interaction between mononaphthalimide spermidine (MINS) and bovine serum albumin (BSA). *J. Photochem, Photobiol. B, Biol*. **2015**, *142*, 103-109, https://doi.org/10.1016/j.jphotobiol.2014.10.013 .
86. Xu, H.; Yao, N.; Xu, H.; Wang, T.; Li, G.; Li, Z. Characterization of the interaction between eupatorin and bovine serum albumin by spectroscopic and molecular modeling methods. *Int. J. Mol. Sci* 2013, *4*, 14185-14203, https://doi.org/10.3390/ijms140714185.
87. Siddiqui, S.; Ameen, F.; Kausar, T.; Nayeem, S. M.; Rehman, S. U.; Tabish, M. Biophysical insight into the binding mechanism of doxofylline to bovine serum albumin: An *in vitro* and *in silico* approach. *Spectrochim. Acta A Mol. Biomol. Spectrosc* **2021,** *249*, 119296, https://doi.org/10.1016/j.saa.2020.119296.
88. Gu, J.; Huang, X.; Ma, Y.; Sun, X. Spectroscopic study on the separate and simultaneous interaction of nicotinic and its metabolite to bovine serum albumin. *J. Mol. Liq* **2022**, *358*, 119106, https://doi.org/10.1016/j.molliq.2022.119106 .
89. Xia, Y.; Xiong, Y.; Lim, B.; Skrabalak, S. E. Shape-controlled synthesis of metal nanocrystals: simple chemistry meets complex physics. *Angew. Chem. Int. Ed* **2009**, *48*, 60-103. https://doi.org/10.1002/anie.200802248 .
90. Idowu, M.; Lamprecht, E.; Nyokong, T. Interaction of water-soluble thiol capped CdTe quantum dots and bovine serum albumin. *J. Photoch. Photobio. A* **2008**, *198*, 7-12, https://doi.org/10.1016/j.jphotochem.2008.02.008.
91. Rao, W.; Li, Q.; Wang, Y.; Li, T.; Wu, L. Comparison of photoluminescence quantum yield of single gold nanobipyramids and gold nanorods. *ACS Nano* **2015**, *9*, 2783-2791, https://doi.org/10.1021/nn506689b.
92. Moreno, F.; Cortijo, M.; Jimenez, J. G. Interaction of acrylodan with human serum albumin. A fluorescence spectroscopic study. *Photochem. Photobiol* **1999**, *70*, 695-700, https://doi.org/10.1111/j.1751-1097.1999.tb08272.x.
93. Kathiravan, A.; Renganathan, R. Interaction of colloidal TiO_2 with bovine serum albumin: a fluorescence quenching study. *Colloid. Surface. A* **2008**, *324*, 176-180, https://doi.org/10.1016/j.colsurfa.2008.04.017.
94. Guo, C. X.; Yang, H. B.; Sheng, Z. M.; Lu, Z. S.; Song, Q. L.; Li, C. M. Layered graphene/quantum dots for photovoltaic devices. *Angew. Chem. Int. Ed* **2010**, *49*, 3014-3017, https://doi.org/10.1002/anie.200906291.
95. Medintz, I. L.; Uyeda, H. T.; Goldman, E. R.; Mattoussi, H. Quantum dot bioconjugates for imaging, labelling and sensing. *Nat. Mater* **2005**, *4*, 435-446, https://doi.org/10.1038/nmat1390.
96. Kathiravan, A.; Anandan, S.; Renganathan, R. Interaction of colloidal TiO_2 with human serum albumin: A fluorescence quenching study. *Colloid. Surface. A* **2009**, *333*, 91-95, https://doi.org/10.1016/j.colsurfa.2008.09.027.
97. Prasad, A. R.; Basheer, S. M.; Gupta, I. R.; Elyas, K. K.; Joseph, A. Investigation on bovine serum albumin (BSA) binding efficiency and antibacterial activity of ZnO nanoparticles. *Mater. Chem. Phys* **2020**, *240*, 122115, https://doi.org/10.1016/j.matchemphys.2019.122115.
98. Ravindran, A.; Singh, A.; Raichur, A. M.; Chandrasekaran, N.; Mukherjee, A. Studies on interaction of colloidal Ag nanoparticles with bovine serum albumin (BSA). *Colloids Surf. B* **2010**, *76*, 32-37, https://doi.org/10.1016/j.colsurfb.2009.10.005.
99. Hao, C.; Xu, G.; Feng, Y.; Lu, L.; Sun, W.; Sun, R. Fluorescence quenching study on the interaction of ferroferric oxide nanoparticles with bovine serum albumin. *Spectrochim. Acta A Mol. Biomol. Spectrosc* **2017**, *184*, 191-197, https://doi.org/10.1016/j.saa.2017.05.004.
100. Esfandfar, P.; Falahati, M.; Saboury, A. Spectroscopic studies of interaction between CuO nanoparticles and bovine serum albumin. *J. Biomol. Struct. Dyn* **2016**, *34*, 1962-1968, https://doi.org/10.1080/07391102.2015.1096213.
101. Jose, P. A.; Sankarganesh, M.; Raja, J. D.; Sakthivel, A.; Annaraj, J.; Jeyaveeramadhavi, S.; Girija, A. Spectrophotometric and fluorimetric detection of DNA/BSA interaction, antimicrobial, anticancer, antioxidant and catalytic activities of biologically active methoxy substituted pyrimidine-ligand capped

copper nanoparticles. *Spectrochim. Acta A Mol. Biomol. Spectrosc* **2022**, *267*, 120454, https://doi.org/10.1016/j.saa.2021.120454.
102. Bhogale, A.; Patel, N.; Mariam, J.; Dongre, P. M.; Miotello, A.; Kothari, D. C. Comprehensive studies on the interaction of copper nanoparticles with bovine serum albumin using various spectroscopies. *Colloids Surf. B* **2014**, *113*, 276-284, https://doi.org/10.1016/j.colsurfb.2013.09.021.
103. Boulos, S. P.; Davis, T. A.; Yang, J. A.; Lohse, S. E.; Alkilany, A. M.; Holland, L. A.; Murphy, C. J. Nanoparticle–protein interactions: a thermodynamic and kinetic study of the adsorption of bovine serum albumin to gold nanoparticle surfaces. *Langmuir*, **2013**, *29*, 14984-14996, https://doi.org/10.1021/la402920f.
104. Chakraborti, S.; Joshi, P.; Chakravarty, D.; Shanker, V.; Ansari, Z. A.; Singh, S. P.; Chakrabarti, P. Interaction of polyethyleneimine-functionalized ZnO nanoparticles with bovine serum albumin. *Langmuir* **2012**, *28*, 11142-11152, https://doi.org/10.1021/la3007603.
105. Jose, P. A.; Sankarganesh, M.; Raja, J. D.; Senthilkumar, G. S.; Asha, R. N.; Raja, S. J.; Sheela, C. D. Bio-inspired nickel nanoparticles of pyrimidine-Schiff base: *In vitro* antiancer, BSA and DNA interactions, molecular docking and antioxidant studies. *J. Biomol. Struct. Dyn* **2021**, 1-15, https://doi.org/10.1080/07391102.2021.1947382.
106. Hashemnia, S.; Zarei, H.; Mokhtari, Z.; Mokhtari, M. H. An investigation of the effect of PVP-coated silver nanoparticles on the interaction between clonazepam and bovine serum albumin based on molecular dynamics simulations and molecular docking. *J. Mol. Liq* **2021**, *323*, 114915, https://doi.org/10.1016/j.molliq.2020.114915.
107. Mariam, J.; Dongre, P. M.; Kothari, D. C. Study of interaction of silver nanoparticles with bovine serum albumin using fluorescence spectroscopy. *J. Fluoresc* **2011**, *21*, 2193, https://doi.org/10.1007/s10895-011-0922-3.
108. Shi, X.; Li, D.; Xie, J.; Wang, S.; Wu, Z. Chen, H. Spectroscopic investigation of the interactions between gold nanoparticles and bovine serum albumin. *Chin. Sci. Bull* **2012**, *57*, 1109-1115, https://doi.org/10.1007/s11434-011-4741-3.
109. Wellington, K. W.; Understanding cancer and the anticancer activities of naphthoquinones-a review. *RSC Adv* **2015**, *5*, 20309-20338, https://doi.org/10.1039/C4RA13547D .
110. Pinto, A. V.; de Castro, S. L. The trypanocidal activity of naphthoquinones: a review. *Molecules* **2009**, *14*, 4570-4590, https://doi.org/10.3390/molecules14114570.
111. Macias-Ruvalcaba, N.; Cuevas, G.; Gonzalez, I.; Aguilar-Martínez, M. Relationship between molecular structure and electron targets in the electro reduction of benzocarbazolediones and anilinenaphthoquinones. Experimental and theoretical study. *J. Org. Chem* **2002**, *67*, 3673-3681, https://doi.org/10.1021/jo011083k.
112. Verma, R. P. Anti-cancer activities of 1, 4-naphthoquinones: a QSAR study. Anti-Cancer agents in medicinal chemistry (Formerly Current Medicinal Chemistry-Anti-Cancer Agents). **2006**, *6*, 489-499, https://doi.org/10.2174/187152006778226512.
113. Bolton, J. L.; Trush, M. A.; Penning, T. M.; Dryhurst, G.; Monks, T. J. Role of quinones in toxicology. *Chem. Res. Toxicol* **2000**, *13*, 135-160, https://doi.org/10.1021/tx9902082.
114. Rodriguez, C. E.; Shinyashiki, M.; Froines, J.; Yu, R. C.; Fukuto, J. M.; Cho, A. K. An examination of quinone toxicity using the yeast Saccharomyces cerevisiae model system. *Toxicology* **2004**, *201*, 185, https://doi.org/10.1016/j.tox.2004.04.016.
115. Song, C. X.; Labhasetwar, V.; Murphy, H.; Qu, X.; Humphrey, W. R.; Shebuski, R. J.; Levy, R. J. Formulation and characterization of biodegradable nanoparticles for intravascular local drug delivery. *J. Control. Release* **1997**, *43*, 197-212, https://doi.org/10.1016/S0168-3659(96)01484-8.
116. Jarabak, R.; Harvey, R. G.; Jarabak, J. Redox cycling of polycyclic aromatic hydrocarbon o-quinones: metal ion-catalyzed oxidation of catechols bypasses inhibition by superoxide dismutase. *Chem.-Biol. Interact* **1998**, *115*, 201-212, https://doi.org/10.1016/s0009-2797(98)00070-2.
117. Shahabadi, N.; Maghsudi, M.; Kiani, Z.; Pourfoulad, M. Multispectroscopic studies on the interaction of 2-tert-butylhydroquinone (TBHQ), a food additive, with bovine serum albumin. *Food Chemistry* **2011**, *124*, 1063-1068, https://doi.org/10.1016/j.foodchem.2010.07.079.
118. Satheshkumar, A.; Elango, K. P. Spectroscopic and molecular docking studies on the charge transfer complex of bovine serum albumin with quinone in aqueous medium and its influence on the ligand binding property of the protein. *Spectrochim. Acta A Mol. Biomol. Spectrosc* **2014**, *130*, 337-343, https://doi.org/10.1016/j.saa.2014.03.108.

119. Suganthi, M.; Elango, K. P. Synthesis, characterization and serum albumin binding studies of vitamin K3 derivatives. *J. Photochem. Photobiol. B, Biol* **2017**, *166*, 126-135, https://doi.org/10.1016/j.jphotobiol.2016.11.016.
120. Kosiha, A.; Parthiban, C.; Elango, K. P. Metal (II) complexes of bioactive aminonaphthoquinone-based ligand: synthesis, characterization and BSA binding, DNA binding/cleavage, and cytotoxicity studies. *J. Coord. Chem* **2018**, *71*, 1560-1574, https://doi.org/10.1080/00958972.2018.1461846.
121. Kosiha, A.; Lo, K. M.; Parthiban, C.; Elango, K. P. Studies on the interaction of mononuclear metal (II) complexes of amino-naphthoquinone with bio-macromolecules., *Mater. Sci. Eng. C* **2019**, *94*, 778-787, https://doi.org/10.1016/j.msec.2018.10.021.
122. Suganthi, M.; Elango, K. P. Spectroscopic and molecular docking studies on the albumin-binding properties of metal (II) complexes of Mannich base derived from lawsone. *J. Biomol. Struct. Dyn* **2019**, *37*, 1136-1145, https://doi.org/10.1080/07391102.2018.1450788.
123. Nariya, P.; Shukla, F.; Vyas, H.; Devkar, R.; Thakore, S. Synthesis, characterization, DNA/BSA binding and cytotoxicity studies of Mononuclear Cu (II) and V (IV) complexes of Mannich bases derived from Lawsone. *J. Mol. Struct* **2022**, *1248*, 131508, https://doi.org/10.1016/j.molstruc.2021.131508.
124. Kosiha, A.; Parthiban, C.; Elango, K. P. Synthesis, characterization and DNA binding/cleavage, protein binding and cytotoxicity studies of Co (II), Ni (II), Cu (II) and Zn (II) complexes of aminonaphthoquinone. *J. Photochem. Photobiol. B, Biol* **2017**, *168*, 165, https://doi.org/10.1016/j.jphotobiol.2017.02.010.
125. Anjomshoa, M.; Torkzadeh-Mahani, M.; Shakeri, M.; Adeli-Sardou, M. The Zn (II) nanocomplex: Sonochemical synthesis, characterization, DNA-and BSA-binding, cell imaging, and cytotoxicity against the human carcinoma cell lines. *J. Fluoresc* **2016**, *26*, 1007-1020, https://doi.org/10.1007/s10895-016-1788-1.
126. Pham, T. P. T.; Cho, C. W.; Yun, Y. S. Environmental fate and toxicity of ionic liquids: a review. *Water research* **2010**, *44*, 352-372, https://doi.org/10.1016/j.watres.2009.09.030.
127. Xia, L.; Li, X.; Wu, Y.; Hu, B.; Chen, R. Ionic liquids based single drop microextraction combined with electrothermal vaporization inductively coupled plasma mass spectrometry for determination of Co, Hg and Pb in biological and environmental samples. *Spectrochim. Acta B: At. Spectrosc* **2008**, *63*, 1290-1296, https://doi.org/10.1016/j.sab.2008.09.018.
128. Kelley, D.; McClements, D. J. Interactions of bovine serum albumin with ionic surfactants in aqueous solutions. *Food Hydrocoll* **2003**, *17*, 73-85, https://doi.org/10.1016/S0268-005X(02)00040-1.
129. Ruiz-Peña, M.; Oropesa-Nuñez, R.; Pons, T.; Louro, S. R. W.; Pérez-Gramatgesa, A. Physico-chemical studies of molecular interactions between non-ionic surfactants and bovine serum albumin. *Col-Surfaces B: Biointerfaces* **2010**, *75*, 282-289, https://doi.org/10.1016/j.colsurfb.2009.08.046.
130. Valstar, A.; Almgren, M.; Brown, W. The interaction of bovine serum albumin with surfactants studied by light scattering. *Langmuir* **2000**, *16*, 922, https://doi.org/10.1021/la990423i.
131. Kuznetsova, D. A.; Gabdrakhmanov, D. R.; Lukashenko, S. S.; Voloshina, A. D.; Sapunova, A. S.; Kashapov, R. R.; Zakharova, L. Y. Self-assembled systems based on novel hydroxyethylated imidazolium-containing amphiphiles: Interaction with DNA decamer, protein and lipid. *Chem. Phys. Lipids* **2019**, *223*, 104791, https://doi.org/10.1016/j.chemphyslip.2019.104791.
132. Kuznetsova, D. A.; Gabdrakhmanov, D. R.; Lukashenko, S. S.; Faizullin, D. A.; Zuev, Y. F.; Nizameev, I. R.; Kadirov, M. K.; Kuznetsov, D. M.; Zakharova, L. Y. Interaction of bovine serum albumin with cationic imidazolium-containing amphiphiles bearing urethane fragment: Effect of hydrophobic tail length. *J. Mol. Liq* **2020**, *307*, 113001, https://doi.org/10.1016/j.molliq.2020.113001.
133. Huang, R.; Zhang, S.; Pan, L.; Li, J.; Liu, F.; Liu, H. Spectroscopic studies on the interactions between imidazolium chloride ionic liquids and bovine serum albumin. *Spectrochim. Acta A Mol. Biomol. Spectrosc* **2013**, *104*, 377-382, https://doi.org/10.1016/j.saa.2012.11.087.
134. Zhu, L. Y.; Li, G. Q.; Zheng, F. Y. Interaction of bovine serum albumin with two alkylimidazolium-based ionic liquids investigated by microcalorimetry and circular dichroism. *J. Biophys. Chem* **2011**, *2*, 146-151, https://doi.org/10.4236/jbpc.2011.22018.
135. Shu, Y.; Liu, M.; Chen, S.; Chen, X.; Wang, J. New insight into molecular interactions of imidazolium ionic liquids with bovine serum albumin. *J. Phys. Chem. B* **2011**, *115*, 12306-12314, https://doi.org/10.1021/jp2071925.
136. Wang, X.; Liu, J.; Sun, L.; Yu, L.; Jiao, J.; Wang, R. Interaction of bovine serum albumin with ester-functionalized anionic surface-active ionic liquids in aqueous solution: a detailed physicochemical and conformational study. *J. Phys. Chem. B* **2012**, *116*, 12479-12488, https://doi.org/10.1021/jp307516a.

137. Satish, L.; Millan, S.; Sahoo, H. Spectroscopic insight into the interaction of bovine serum albumin with imidazolium-based ionic liquids in aqueous solution. *J. Lumin* **2017**, *32*, 695-705, https://doi.org/10.1002/bio.3239.
138. Samarkina, D. A.; Gabdrakhmanov, D. R.; Lukashenko, S. S.; Khamatgalimov, A. R.; Zakharova, L. Y. Aggregation capacity and complexation properties of a system based on an imidazole-containing amphiphile and bovine serum albumin. *Russ. J. Gen. Chem* **2017**, *87*, 2826-2831, https://doi.org/10.1134/S1070363217120118.
139. Samarkina, D. A.; Gabdrakhmanov, D. R.; Lukashenko, S. S.; Nizameev, I. R.; Kadirov, M. K.; Zakharova, L. Y. Homologous series of amphiphiles bearing imidazolium head group: Complexation with bovine serum albumin. *J. Mol. Liq* **2019**, *275*, 232-240, https://doi.org/10.1016/j.molliq.2018.11.082.
140. Gospodarczyk, W.; Kozak, M. Interaction of two imidazolium gemini surfactants with two model proteins BSA and HEWL. *Colloid Polym. Sci* **2015**, *293*, 2855-2866, https://doi.org/10.1007/s00396-015-3671-z.